# Resistive Matching using an AC Boost Converter

## for Efficient Ultrasonic Wireless Power Transfer

M.C. Bisschop

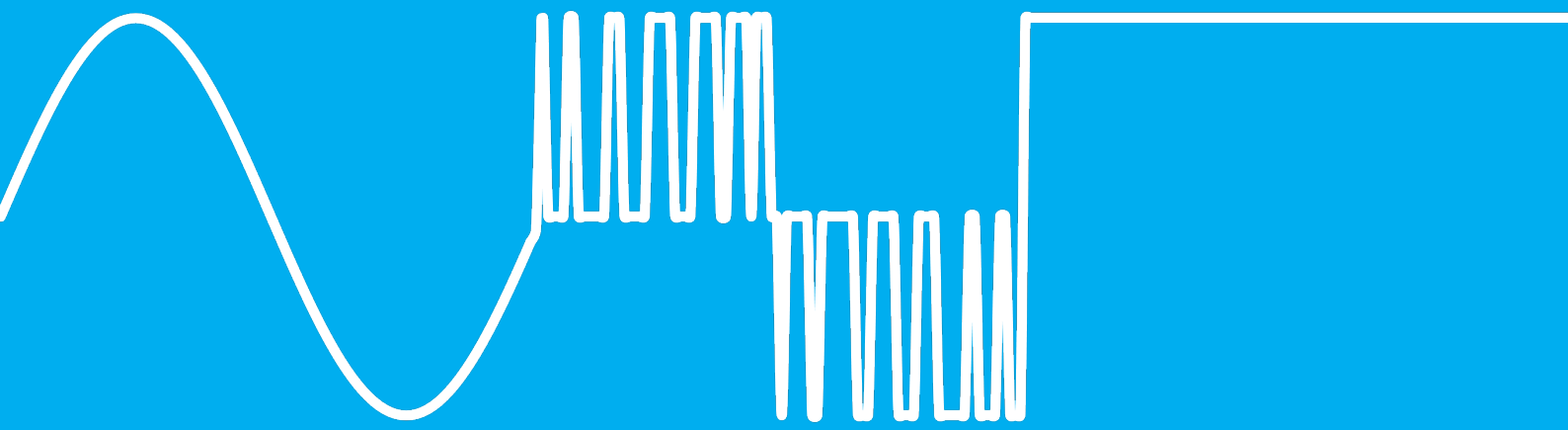

TU Delft

# Resistive Matching using an AC Boost Converter

## for Efficient Ultrasonic Wireless Power Transfer

by

M.C. Bisschop

to obtain the degree of Master of Science
in Electrical Engineering
at the Delft University of Technology,
to be defended publicly on Friday May 24, 2019 at 3:00 PM.


| | | |
|---|---|---|
| Student number: | 4171101 | |
| Thesis committee: | Prof. dr. ir. W.A. Serdijn, | TU Delft, supervisor |
| | Dr. ir. M.A.P. Pertijs, | TU Delft |
| | Dr. V. Valente, | University College London & TU Delft |




TU Delft

# Abstract

Implantable Medical Devices (IMDs) could fulfill many different functions in the human body. Batteries have always been the main power source of these devices. Batteries have some drawbacks, the biggest one being the replacement of IMDs with fully discharged batteries. In this thesis a wireless power transfer system, with a receiving power conversion system with a maximum volume of $10$ mm$^3$, is proposed for IMDs implanted at more than $10$ cm deep.

Ultrasonic wireless power transfer to IMDs could enable scaling down the devices to dimensions less than $1$ cm. Compared with the electromagnetic far-field and near-field wireless power transfer methods, the power throughput to the IMD is much higher.

Piezo-electric elements could be used to perform the acoustic to electric energy conversion. With the Butterworth-Van Dyke modeling technique, the ultrasonic wireless power transfer link could be characterized. Maximum acoustic intensity at the receiving piezo-electric element is assumed because of the high efficiency and the possible methods to focus the waves from the transmitter at a certain point in the human body. An electrical storage element is assumed because of fluctuations both in received and used power.

As the piezo-electric receiver outputs sinusoidal voltage and current waveforms, and the electrical storage element requires DC voltage, the signal requires significant processing for maximum power transfer. A perfect complex conjugate match between the piezo-electric receiver and the power conversion circuit is required for maximum power transfer as well. Two different methods which are used in prior art to achieve maximum power transfer are presented in this thesis, and one new method is developed. The standard method, which is used often in literature, does not include any special processing by means of impedance transformations and is therefore only efficient around one power level operating point. The varying frequency method varies the frequency so as to vary the piezo resistance and match it to the power conversion systems resistance. The piezo inductance varies with the varying piezo resistance, and is canceled out by tunable capacitor banks. A DC boost converter is required for high efficiency to the electric storage element. This method has many drawbacks, among which the continuous communication back to the transmitter to close the loop, which is consuming power and adding delay. The newly proposed method is the AC boost method. The AC voltage of the piezo-electric receiver is transformed into a pulse width modulated square wave voltage, so all power could go through the rectifier and into the storage element. A continuous resistive match is made between the AC boost converter and the piezo-electric element, ensuring maximum power transfer.

This new method is validated by performing electric circuit simulations. Circuits are designed for the simulations that are comparable because of using the same piezo-electric element, rectifier, and storage element. The simulations show that it is the most efficient method for a wide load power range of $10\,\mu$W to $5\,$mW. The standard method is as efficient but only at a small range at high power level. The varying frequency method is much more complex and has, therefore, lower power efficiency at high power levels whereas at low power levels it has the same power efficiency.

# Acknowledgements

I am grateful to many persons who helped me during this project. First of all, I would like to thank Wouter Serdijn. From the very beginning of my studies at Delft University of Technology, you inspired me to study circuit theory. I am grateful for your open way of supervision, by asking questions and without pushing. Our meetings often inspired me and it accelerated my thinking process.

I would like to say thanks to the Bioelectronics group. Thank you for the experience of being part of this group. This thesis is brought to a higher level and encouraged by many conversations, presentations, reviews, and discussions, thank you all.

Further, I would like to express my gratitude towards my family and friends. Many stories I have told you about my project, and it seems that electronic theory is often a challenge to understand. I want to thank everybody for all the interest and encouragement for this project. Johanna, I would like to thank for your everlasting love and for being there for me. Parents, I would like to thank you for your unconditional support and all the opportunities you gave me.

Lastly, I would like to praise my heavenly Father for all inspiration, love, and curiosity.

*Marc Bisschop*
*Delft, May 2019*

# Contents

# 1 Introduction

## 1.1. Problem definition

In the human body many biological processes are regulated by electrical signals. For treatment of diseases or restoration of biological functioning bioelectronic medicine could be used. These Implantable Medical Devices (IMDs) impose an electrical signal on the nerves or muscles to influence the biological processes. In the field of IMDs, the interest in bioelectronic medicine is growing because the advancing technology is enabling more and more applications, such as cochlear implants or glucose monitors [1, 2].

Batteries have always been the main power source of IMDs. Batteries, however, have some huge drawbacks. The size of the implant is often determined by the required battery capacity. Whereas the electronics grow smaller every year, the battery size is barely decreasing. The capacity per volume is not increasing fast and restrictions in safety and lifetime pose challenges to powering IMDs. The moment the battery is empty, the whole implant has to be replaced. This gives a potential health risk because of intensive surgery [2, 3].

In this introduction we will first look into the dimensions of IMDs and the proposed powering approach. Next, an application example will be described. This chapter concludes with the research questions and thesis outline.

### 1.1.1. Dimensions

The dimensions of the IMDs should be in the range of millimeters to be widely applicable in the human body at different organs. Most organs have centimeter-size dimensions. IMDs should be smaller than the organs for not disturbing the body and its processes, and being able to be implanted at difficult locations. Current IMDs could be made small enough to operate at nearly every place in the human body. A size of some cubical millimeters is possible when no battery is needed and the other functionality of the IMD is small enough as well [4].

### 1.1.2. Powering approach

Multiple different solutions to the battery powering problem are proposed. The average required power of IMDs is in the range of µWs to some mWs, depending on the application. Constant stimulation or constant communication requires most power [5]. Two different solution approaches are possible: harvesting power from the environment around it, and wireless power transfer from an outside source. Motion powered energy harvesters, thermal energy harvesters, and cuel cell energy harvesters are proposed. However, most of these harvesting projects are in the research phase. Often the energy densities are too low or the harvesting is unreliable on the longer term [2]. For wireless power transfer, the inductive coupled coils are the most widespread method. Recently, ultrasound is demonstrated as a potential wireless power transfer method as well [3]. In this thesis the wireless powering method for IMDs will be researched.

The human body is inhomogeneous as there are multiple different materials involved in the body with each its own characteristics. The dielectric properties are different but also the stiffness or the density. Further, even in one body-material-type there is inhomogeneity. Wireless powering of an IMD therefore has some challenges. The power throughput is not constant, due to the inhomogeneity and

movement, or body processes. Wireless power is attenuated over distance because of absorption and spreading of the wireless power waves, so deep in the body much power is lost. The lost power is transformed into heat which is bounded by safety levels. Due to these challenges there is still not a good system for wireless powering IMDs deep in the body.

The aim of this project is to come up with a method for maximum power transfer to a $10$ cm deep implanted IMD, where the receiving power conversion system has a maximum volume of $10$ mm$^3$, so as to enabling a total device with all dimensions smaller than $1$ cm.

### 1.1.3. Application example: diabetes treatment

Deep inside the human body, the pancreas is located; it is behind the stomach and, therefore, difficult to reach in surgery. See Figure 1.1 for its location. It is part of the digestive system and responsible for making insulin to control the blood sugar level.

In people who are suffering from diabetes the pancreas is malfunctioning and the blood sugar level is regularly too high. Diabetes Mellitus Type 1 is the result of malfunctioning beta cells who are responsible for producing enough insulin. When the response of cells to produced insulin fails it is called Type 2. In animal models it is shown that electrical stimulation of the pancreas could lead to more insulin secretion for patients with Type 1 diabetes. The closer to the pancreas the stimulation happens the less other organs will be influenced by the stimulation. A tiny device implanted for decades on the pancreas, that measures blood glucose levels and insulin levels can thus control the insulin level by stimulating the pancreas [7, 8].

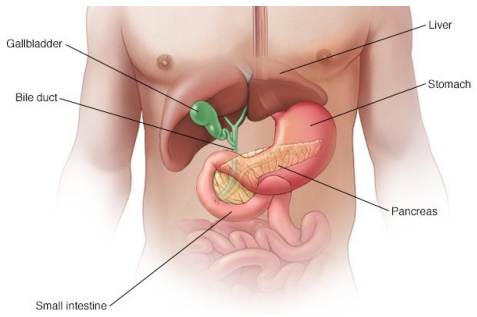


Figure 1.1: The location of the pancreas and the surrounding organs. Figure taken from [6].

## 1.2. Research questions and thesis outline

The following main research question is defined for this project:

**Main Question** **How could maximum power transfer be achieved with wireless power transfer to a 10 cm deep implanted biomedical device?**

This question is divided in six sub-questions. Every chapter focuses on one question. The first question that has to be answered in Chapter 2 is:

**Question 1** What are the wireless power transfer methods and which is the best suitable for powering an IMD at $10$ cm deep?

The selected wireless power transfer method will be ultrasonic powering, so next we study this ultrasonic wireless power transfer link in Chapter 3:

**Question 2** How could the ultrasonic wireless power transfer link be characterized?

For maximum power transfer to the load, different methods are studied in Chapter 4, two conventional methods and one newly developed method:

**Question 3** What methods could be employed for maximum power transfer (MPT) to the electrical storage element?

These methods are made comparable by designing an electrical circuit for simulation, this is described in Chapter 5:

**Question 4** How could the MPT methods be compared in electrical simulation?

The results of the comparison of the maximum power transfer methods are addressed in Chapter 6:

**Question 5** What are the results of the comparison of the MPT methods?

In the discussion, Chapter 7, the validity is discussed and the future possibilities are studied:

**Question 6** What is the validity of the approach and of the results, what are its limitations, and how could the AC boost method be utilized?

The final conclusions to the main research question will be drawn in the last chapter, Chapter 8. Also the contributions and future work will be addressed here.

In the appendix the paper written for the “Wireless Power Transfer Conference 2019” is included.

# 2

# Wireless power transfer comparison

Wireless Power Transfer (WPT) is the transfer of usable energy from a power source to a load without using wires between them. For IMDs the load is an electronic load. In this chapter the following question will be answered:

***Question 1**: What are the wireless power transfer methods and which is the best suitable for powering an IMD at* $10$ *cm deep?*

We are looking to a place $10$ cm deep in the body and the maximum size of the power conversion system will be $10$ mm$^3$.

In this chapter, three wireless power transfer techniques will be investigated. First these will be introduced. The discussion of the important properties for total power throughput follows. From this discussion, a conclusion will be drawn about the most suitable wireless power transfer technique.

## 2.1. General block diagram of wireless power transfer

In Figure 2.1 the general block diagram of wireless power transfer is shown; as can be seen, it is symmetrical. The power comes from an electric storage element on the outside of the body and is transformed into AC power that drives a transmitter (TX). Via the medium, that is the body, the wireless power is transferred to the receiver (RX). Here it is converted into AC electrical power again, an AC to DC converter (e.g. rectifier) makes DC power that could be stored on a capacitor or in a small battery. After this the power could be used by an IMD.

## 2.2. Three wireless power transfer techniques

There are currently two different ways of wireless power transfer: electromagnetic waves and pressure waves.

Electromagnetic waves are currently mostly used for wireless power transfer. The near-field electromagnetic wireless power transfer with inductive coupling is utilized a lot. Wireless power transfer with electromagnetic waves in the far-field at radio frequencies via antennas is also used.

Pressure waves can be made with ultrasound. Ultrasonic wireless power transfer is utilized less than electromagnetic wireless power transfer but there is a growing scientific interest in this method [9]. Figure 2.2 shows the potential usability of ultrasound as a powering method [4]. Ultrasonic wireless power transfer has the ability to get more power deeper into the body than powering the device with radio frequencies. At the same time it is smaller than devices with near-field electromagnetic powering.

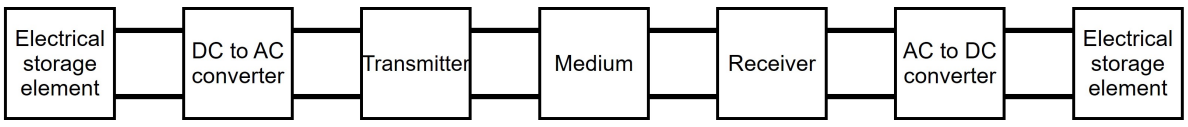


Figure 2.1: General block diagram for wireless power transfer.

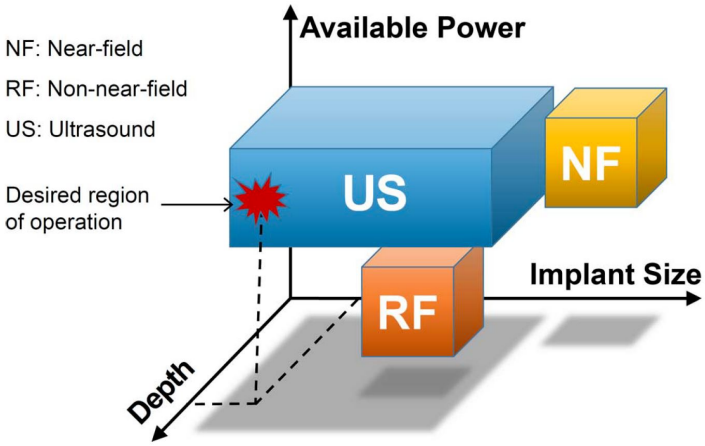


Figure 2.2: The different wireless powering techniques shown in a conceptual diagram. The desired region of operation is indicated. Picture taken from [4].

Three powering methods are used for powering biomedical implants: near-field electromagnetic, far-field electromagnetic and ultrasonic. In this section, these powering methods will be compared to each other.

### 2.2.1. Near-field electromagnetic

Near-field resonant inductive coupling is the oldest technique for wireless power transfer in bioelectronic medicine. It is also know as magnetostatic wireless power transfer as the power is transferred through magnetic fields. The United States Food and Drug Administration (FDA) has approved some implantable devices that employ this technique. Until now the applications are limited: for example cochlear implants that are located in the head against the skin, or retinal implants in the eye [2, 10]. So distances in these applications are short.

The principle utilized in this powering technique is magnetic induction. See Figure 2.3. The primary coil ($L_{tx}$) is located outside the body and driven by a sinusoidal current. This coil transmits a time-varying magnetic field. An electromotive force (emf) is induced in a receiving coil ($L_{rx}$) in the body by the time varying magnetic field. This power is then provided to the load. The induced emf $\mathcal{E}$ is given by [10]:

$$\mathcal{E} = \oint_{\partial\Sigma} \vec{E} \cdot d\vec{l} = -\frac{d}{dt} \int_{\Sigma} \vec{B} \cdot d\vec{A} \tag{2.1}$$

where $\Sigma$ is the surface bounded by $L_{rx}$, $\vec{E}$ is the electric field, $d\vec{l}$ is the vector element of the contour $\mathcal{E}\Sigma$, $\vec{B}$ is the magnetic flux density through $L_{rx}$, and $d\vec{A}$ is the area vector element of surface $\Sigma$.

Maximizing the power through this wireless link involves [10]:

1. High magnetic field strength
2. High rate of change of the magnetic field
3. High flux linkage between $L_{rx}$ and $L_{tx}$

High flux linkage needs short distance for high coupling.

### 2.2.2. Far-field electromagnetic

In Figure 2.4 the far-field electromagnetic wireless power transfer is shown. The energy could be focused so quite a high efficiency is possible. In the far-field, the transmitting and receiving antenna are a great distance away from each other: $D \geq 2d^2/\lambda$ and $\lambda = v/f$, where $d$ is the largest antenna dimension in m, $\lambda$ is the wavelength of the electromagnetic wave in m, $v$ is the speed of the wave in m/s and $f$ is the frequency of the wave in Hz. An alternating current creates a travelling electromagnetic wave at the TX antenna. This wave is in the far-field region a plane wave. The frequency is often chosen to be in the GHz-range for mm-sized applications, which makes the total system less efficient than the near-field coupling because of higher tissue and rectification losses for example [10].

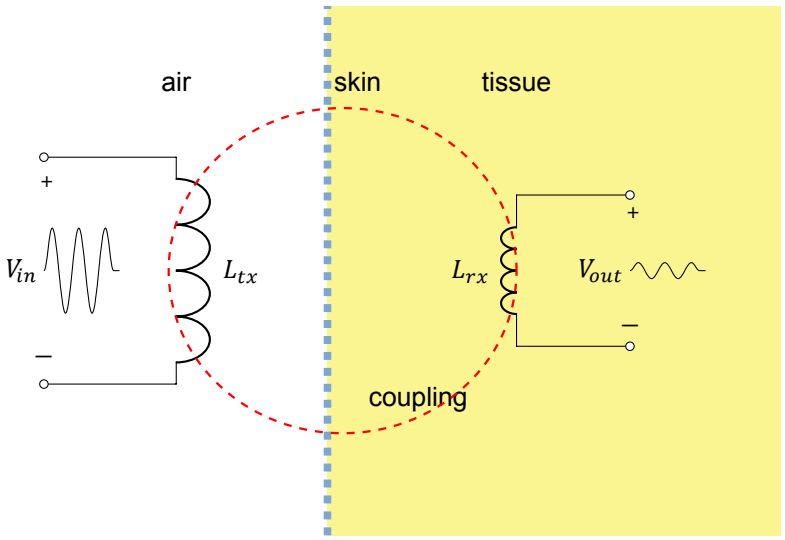


Figure 2.3: near-field inductive coupling wireless power transfer.

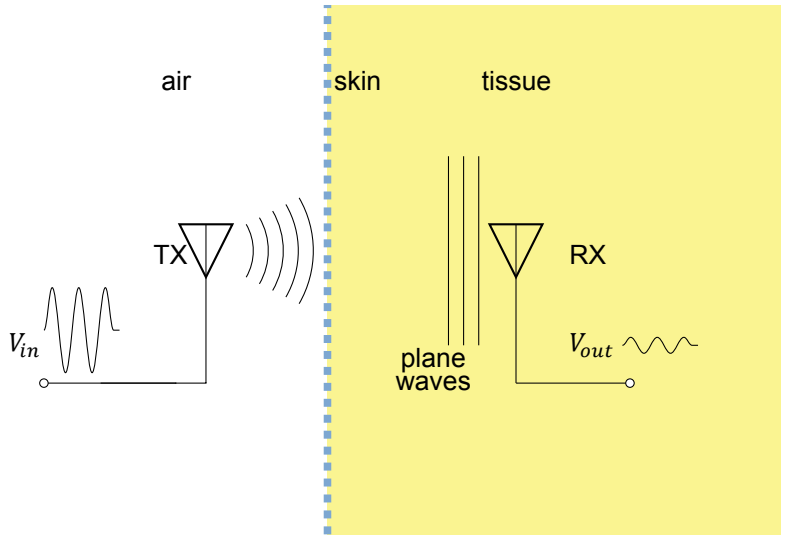


Figure 2.4: far-field electromagnetic wireless power transfer.

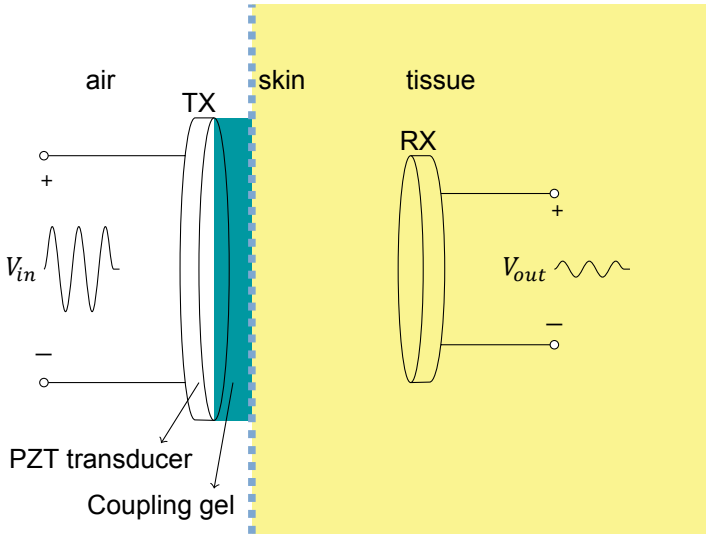


Figure 2.5: Ultrasonic wireless power transfer.

### 2.2.3. Ultrasonic

When using the ultrasonic wireless powering method, sound waves are used that have a frequency higher than human hearing (20 kHz). Sound waves are waves of varying pressure. Figure 2.5 gives insight in an ultrasonic wireless power link. An electrical source drives a transducer (TX) with an alternating current. This makes an acoustic pressure wave. Via a coupling gel the wave travels into the tissue where the receiving transducer is (RX). The pressure wave is transformed here in an alternating electrical voltage, which could be used by the implant.

Ultrasonic wireless power transfer needs a medium to travel through. At the boundaries between different media the difference in acoustic impedances (or velocities) should be as small as possible because the larger the difference the more reflection will occur. The best medium is a homogeneous medium that is perfectly matched to the transducers. Soft tissue is not homogeneous but the acoustic impedance is quite constant. The acoustic wave becomes after the Rayleigh distance a few degrees unfocused, resulting in a decreasing power density [10].

## 2.3. Properties of wireless power transfer

In a wireless power transfer link the following parameters define the total maximum available electrical power at the implanted device:

- Power input limits
- Power attenuation in the tissue
- Power conversion efficiency to usable electrical energy

We will study each of these properties to determine the best method.

### 2.3.1. Power input safety limits

The maximum allowed electromagnetic wave intensity is $10 - 100$ μW$^2$, depending on the frequency and the location in the body [11]. Human tissue is not allowed to heat up more than $1\,^{\circ}$C due to the electromagnetic field [4].

The United States of America Food and Drug Administration (FDA) allows $7.2$ mW/mm$^2$ for diagnostic ultrasound continuously [12]. This is $72$ to $720$ times more than electromagnetic.

Time varying electromagnetic fields induce displacements currents in the tissue. Ultrasonic waves compress the tissue. Compression gives a lower attenuation than the displacement currents give and therefore less heat. Due to less heat this leads to higher safety values [13].

### 2.3.2. Power attenuation

As stated before, ultrasonic waves attenuate less through tissue than electromagnetic waves. Table 2.1 shows the penetration depth in soft tissue of electromagnetic and ultrasonic waves at different frequen-

cies. Penetration depth is the depth at which the power density is attenuated by $e^{-2} = -8.7$dB. For an electromagnetic wave at $3000$ MHz it holds that it has about the same wavelength as an ultrasonic wave at $0.1$ MHz. Here the penetration depth of ultrasonic waves is more than $50$ times better. The assumption for ultrasound is that the attenuation is about $1$ dB/cm·MHz. Literature states $0.8$ to $1$ dB/cm·MHz [3].

Table 2.1: Wavelength and penetration depth for ultrasonic and electromagnetic waves at different frequencies [14, p.23][15]. * linearized result

| | Ultrasonic | | Electromagnetic | |
|---|---|---|---|---|
| Freq (MHz) | $\lambda$ (mm) | pen. depth (mm) | $\lambda$ (mm) | pen. depth (mm) |
| 0.1 | 16* | 870 | | |
| 1 | 1.6 | 87 | 4360 | 913 |
| 10 | 0.16 | 8.7 | 1180 | 216 |
| 100 | | | 270 | 66.6 |
| 1000 | | | 40 | 30 |
| 3000 | | | 14.5 | 16.1 |

### 2.3.3. Power efficiency at mm-size receiver

The better the wavelength matches with the dimensions of the receiver, the higher the power conversion efficiency will be [14]. So the wavelength should be in the mm region for a mm-sized implant:

$$\lambda = \frac{v}{f} \tag{2.2}$$

With $\lambda$ the wavelength in m, $v$ the wave velocity in m/s and $f$ the frequency in Hz.

Table 2.1 shows the wavelengths at different frequencies. For the same penetration depth the wavelength of ultrasonic waves is about $100$ times smaller. Or at mm-wavelength the penetration depth of ultrasonic waves is about $10$ cm where electromagnetic waves have only a penetration depth of a few mm.

Waves in the far-field region are much more isotropic than waves operating in the near-field region. Therefore efficiency is much higher. Ultrasonic wireless power transfer is likely to operate in the far-field region [13].

Antennas often have a wider receiving cross section (aperture) than its area is. Therefore, high efficiency at the receiver is possible. The same holds for ultrasonic transducers; however, to a lesser extent. At high frequencies (GHz-range) the rectification losses will be higher so for the far-field electromagnetic technique this means extra losses [10].

Denisov et al. [3] did simulate the efficiency of near-field electromagnetic wireless power transfer with inductive coupling versus ultrasonic wireless power transfer. Figure 2.6 shows their results. They also simulated with bigger receivers and shorter distances but these are the most important figures. What can be seen in the left graph is that for receiver diameters less than $5$ mm the efficiency of acoustic power transfer is $100 - 1000$ times better than inductive powering at $10$ cm distance. The smaller the diameter, the higher this ratio. In the right graph, it can be seen that the efficiency of acoustic power transfer decays linearly with distance while inductive power transfer shows a more inverse exponential relation. At $10$ cm distance the $5$ mm acoustic receiver is $100$ times more efficient than the $5$ mm inductive receiver. The bigger the distance the more the acoustic power transfer outperforms the inductive power transfer. This is mostly because of the increasingly weaker coupling and the large wavelength [3]. Next to this, the large wavelength cannot be focused to a receiver only. This results in excessive heating and low efficiency [16].

## 2.4. Conclusion

Table 2.2 provides a summary of this chapter. Ultrasonic wireless power transfer has higher power input safety limits. It has a lower attenuation than high-frequency far-field electromagnetic wireless power transfer but is comparable with low-frequency near-field magnetic wireless power transfer. The power efficiency at the receiver for ultrasonic and far-field electromagnetic is about the same where near-field magnetic has a low efficiency because of the weak coupling. Ultrasonic wireless power transfer

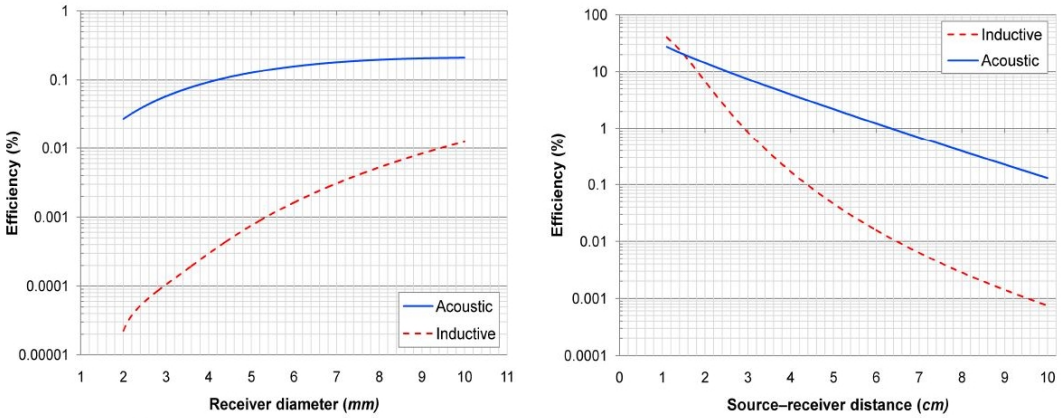


Figure 2.6: Two graphs of efficiency for acoustic and inductive power transfer. Left: efficiency as a function of receiver diameter at 10 cm distance. Right: Efficiency as a function of source-receiver distance for a 5 mm receiver. Picture taken from [3].

outperforms near-field and far-field electromagnetic wireless power transfer for deeply implanted small IMDs. Therefore the ultrasonic wireless power transfer is the best technique to be used. The following chapter will go deeper into the ultrasonic wireless power transfer.

Table 2.2: Summary of the discussed properties of the different wireless power transfer techniques. The far-field electromagnetic technique is used as reference for the other two. + better; 0 not better or worse; - worse.

| Criteria | Near-field electromagnetic | Far-field electromagnetic | Ultrasonic |
|---|---|---|---|
| Power input limits | 0 | 0 | + |
| Power attenuation | + | 0 | + |
| Power efficiency at receiver | - | 0 | 0 |

# 3

# Ultrasonic wireless power transfer link characterization

Now ultrasonic waves are chosen as the wireless power transfer method, this chapter will research the following question:

***Question 2**: How could the ultrasonic wireless power transfer link be characterized?*

The following section introduces the ultrasonic link. Section 3.2 studies the different modeling methods. From these sections a full electric model at the receiver follows in the last section.

## 3.1. Ultrasonic wireless power transfer link

The general block diagram (Figure 2.1) adapted for ultrasonic wireless power transfer can be seen in Figure 3.1. As can be seen the power transfer link is still symmetrical. It starts with some form of DC power and it also ends with DC power. In between are DC to AC converters (or AC to DC), electric to acoustic converters (or acoustic to electric) and a medium. Between every block an impedance match should be made, both in the electrical and the acoustic domain. Often an impedance transformation (IT) has to be done for an impedance match. In this section the electrical transmitter (TX), the acoustic medium, the electrical receiver (RX) and the impedance transformations are introduced.

### 3.1.1. Transmitter

The transmitting transducer transforms electrical power into acoustic power. For this piezo-electric elements are used. Piezo-electricity is a phenomenon whereby electrical charge is generated in some materials when mechanical stress is applied and vice versa [17]. The acoustic power could be focused from an array of transducers outside the body on a spot inside [18, 19]. An energy source outside the body is assumed, for example a large battery that drives the transmitting piezo-element via a DC to AC converter. In this way the complete system is wearable, and more space is available outside the body than inside.

### 3.1.2. Acoustic medium

Not all the energy transmitted by the transmitter is received by the receiver. The following phenomena play a part in the human body [9]:

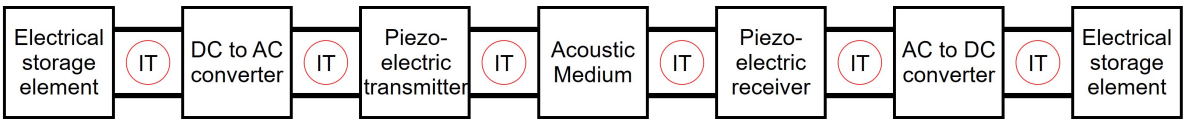


Figure 3.1: General block diagram for ultrasonic power transfer, indicated are all locations were impedance transformations could be made to achieve maximum power transfer between the blocks.

- **Absorption:** the medium is deformed, this costs energy which turns into heat.
- **Scattering:** because of non-uniformity of the medium some waves will not travel in straight lines.
- **Diffraction:** sound waves will bend along corners in the medium.
- **Reflection:** the amount of reflection depends on the acoustic impedance match.
- **Dispersion:** the frequency components in a wave are separated from each other.

Modelling all this behaviour involves extensive techniques. However it comes down to two principles: the ultrasonic waves are attenuated because of losses and part of it is sent in different directions because of the inhomogeneous medium.

The acoustic impedance of a piezoelectric element and tissue has a large difference, respectively $\sim 30$ MRayls and $\sim 1.5$ MRayls [20]. Therefore large reflections at the boundary between the two materials will occur, as will be shown by Equation (3.3). A matching layer at the transmitter of $\lambda/2$ ($= 0.8$ mm at $1$ MHz) or $\lambda/4$ ($= 0.4$ mm at $1$ MHz) will increase the acoustic matching. At the receiver this is also needed.

### 3.1.3. Receiver

At the receiver the acoustic energy is transformed into electrical energy in the piezo-electric element. This could be done at high efficiency ($\sim 1.0$) [21]. The construction of the receiver is important because the backing material of the piezo-electric element should not let the acoustic power leak [18].

At the receiver we want maximum power transfer to an electrical storage. The electrical storage is needed because of fluctuations both in received and used power. The IMD could use the energy of the storage element to power all its functions. The most power consuming functions are stimulation or wireless communication [5].

### 3.1.4. Impedance transformations

Every block in the block diagram could be modelled with a two-port that represents a relation between the incoming and outgoing power at that block. For every block a complex input and output impedance plus a variable voltage source could be defined as in Figure 3.2. The input impedance models the behaviour of all the following blocks. The voltage source together with the output impedance model the behaviour of the previous blocks. The impedances do not necessarily have to be constant. The voltage gain G of a block is also not always constant, for example, a rectifier with diodes provides non-linear voltage gain. The output impedance ($Z_{out}$) of a block should be constantly matched to the input impedance ($Z_{in}$) of the following block for maximum power transfer. The power delivered to the following block is:

$$P_{in} = I^2 Z_{in} = \left(\frac{V_s}{Z_{out} + Z_{in}}\right)^2 \times Z_{in} = \frac{V_s^2}{Z_{out}^2/Z_{in} + 2Z_{out} + Z_{in}} \tag{3.1}$$

A perfect match with maximum power is obtained when:

$$Z_{out} = Z_{in}^* \tag{3.2}$$

where $Z_{in}^*$ is the complex conjugate of $Z_{in}$. Maximum power transfer is not the same as maximum efficiency. The most efficient case would be to have $Z_{out} = 0\ \Omega$ for maximum power at the following block. In our case this is not realistic while the different blocks all will have an output impedance. $Z_{in} = \infty\ \Omega$ gives also efficiency equal to $1$. This is not realistic while the delivered power will be $0$ W there.

The reflected power is [22]:

$$P_{ref} = |\Gamma|^2 P_{out} = \left|\frac{Z_{in} - Z_{out}^*}{Z_{in} + Z_{out}}\right|^2 P_{out} \tag{3.3}$$

$\Gamma$ is called the power wave reflection coefficient. When $Z_{out}$ is equal to $Z_{in}^*$ it gives $P_{ref} = 0$ W. This is the desired situation because reflected power could not be used. Maximum power transfer is obtained because of a perfect match. Reflected power could also lead to interference and damping of incoming new waves in the piezo-element.

A direct match between the $Z_{in}$ and $Z_{out}$ impedances is often not possible. An impedance transformation is needed to obtain the match. For the acoustical domain the reasoning is the same as for the electrical domain. In ultrasonic devices, a matching layer of different material is usually added.

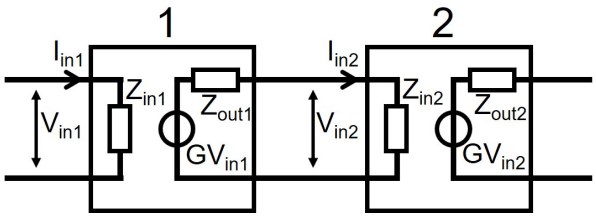


Figure 3.2: For every block in the block diagram a model with an input and output impedance and a voltage source could be defined as in this figure. The input impedance of the following block should be matched to the output impedance of the block in front of it.

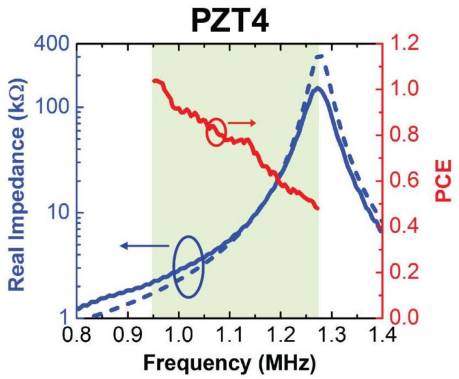


Figure 3.3: Measured power conversion efficiency (PCE, red), measured resistance (blue solid) and simulated resistance (blue dashed) as a function of frequency of a piezo-electric transducer made of PZT4 with dimensions $1.1 \times 1.1 \times 1.5$ mm$^3$. The frequency band between the two resonance frequencies is highlighted in green. Figure taken from [21].

## 3.2. Modeling the ultrasonic wireless power transfer link

Different techniques are used to model the behaviour of ultrasonic waves in (body) material and the combination with the electronics. In this section the most common methods are discussed. First, some remarks on multi-domain modelling will be made. Secondly two extensive modeling techniques, the KLM and the Mason technique, are shown. This is followed by the Butterworth-Van Dyke modeling technique. Finally, the Thévenin equivalency is studied.

### 3.2.1. Multi-domain

Piezo-electric elements perform domain transformations: from the acoustic domain to the electrical domain or vice versa. We are interested in maximum power transfer to the IMD so the Power Conversion Efficiency (PCE) from acoustic to electrical power is an important parameter. Figure 3.3 shows the PCE of a piezo-electric element measured over frequency between the two resonance frequencies. This is $\sim 1.0$ at the lowest resonance frequency, the short circuit resonance frequency. It could be above $1.0$ because the aperture is larger than the area of the transducer. More power is extracted from the acoustic wave than travels through the area of the transducer. The figure also shows the measured and simulated real impedance over frequency, showing equivalence [21]. For matching it is thus important to know the operating frequency and the corresponding impedance.

### 3.2.2. KLM and Mason equivalent circuit model

In the book of Kino [17] the common modeling techniques are described. The KLM (after Krimholtz, Leedom and Matthaei) and Mason model both use a transmission line to model the acoustic energy transfer through the piezoelectric element. A piezo-electric element is modelled with two acoustic ports and one electrical port. See Figure 3.4b for the Mason model and Figure 3.4a for the KLM model. The Mason model requires a negative capacitance at the electrical ports, this was found to be unphysical, and is solved by the KLM model. Models of the acoustic front and back loading of the transducer could be added in series with this transmission line. The electrical energy is extracted (or added) in the middle of the transmission line via an ideal electromechanical transformer. Around the transformer

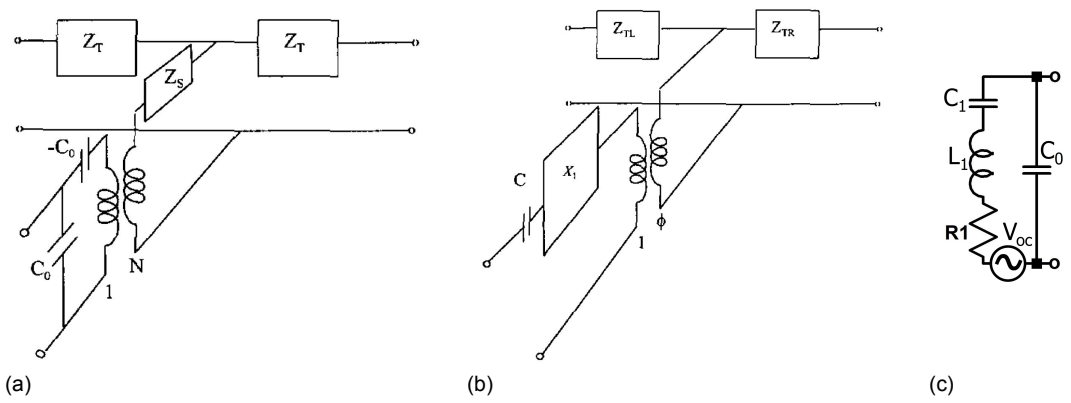


Figure 3.4: (a) KLM and (b) Mason equivalent circuit model. Figures taken from [23]. (c) Butterworth-van Dyke equivalent circuit model.

some components are placed to indicate losses and give the right resonance frequency. The modelling techniques both show equivalence with analytical models [23]. All relevant media could be added to the model: acoustic media to the acoustic ports, and the electrical circuits to the electrical ports, at both the transmitter and receiver.

### 3.2.3. Butterworth-Van Dyke equivalent circuit model

Around the series resonance frequency a lumped element equivalent circuit of the Mason model could be calculated and is shown in Figure 3.4c. This same model is also called the Butterworth-Van Dyke model as they came up with this method. The model is build up of a series RLC circuit and a parallel capacitor $C_0$. It is only valid around resonance frequency [17]. Extra RLC branches could be added to model more resonance frequencies [24].

The open-circuit (series) resonance frequency and short-circuit (parallel anti-)resonance frequency can be calculated as follows [17, 21]:

$$f_{ar} = v/2t \tag{3.4}$$

$$f_r \simeq \sqrt{1 - 8k_{33}^2/\pi^2} f_{ar} \tag{3.5}$$

where $v$ is speed of sound, $t$ is thickness of the transducer and $k_{33}$ is the electro-mechanical coupling coefficient. These frequencies could be multiplied by a correction factor of $1$ to $0.7$ when $W/t \leq 1$ to achieve correct resonance frequencies [21].

In this model, for the length expander mode of the transducer, the passive elements are calculated with [17]:

$$C_0 = \varepsilon_0 \varepsilon_{33}^T (1 - k_{33}^2) WL/t \tag{3.6}$$

$$C_1 = \frac{8k_{33}^2 C_0}{\pi^2 - 8k_{33}^2} \tag{3.7}$$

$$L_1 = \frac{1}{4\pi^2 f_r^2 C_1} \tag{3.8}$$

$$R_1 = \frac{1}{8k_{33}^2 f_r C_0} \frac{Z_F + Z_B}{Z_C} \approx R_r \tag{3.9}$$

With $\varepsilon_{33}^T$ the relative permittivity, $W$ the width of the square device, $Z_C$ the acoustic impedance of the material (Rayls), $Z_F$ the front acoustic loading and $Z_B$ the back acoustic loading and the resonance frequencies the uncorrected values. The model is accurate when $Z_F \ll Z_C$ and $Z_B \ll Z_C$ [21]. In Table 3.1 these properties are shown for PZT4.

For a piezo-electric element made of PZT4 with $t = 1.5$ mm, $W = L = 1.1$ mm, $Z_F = 1.5$ MRayls (tissue) and $Z_B = 400$ Rayls (air) it gives $f_{ar} = 1.27$ MHz and $f_r = 0.99$ MHz with $R_r = 2.48$ kΩ and $R_{ar} = 244$ kΩ. The impedance of this equivalent circuit model is plotted in Figure 3.5 with correction

Table 3.1: Properties of PZT4 [17, 21]

| Property | Value |
|---|---|
| Sound velocity $v$ (m/s) | 4100 |
| Acoustic impedance $Z_C$ (Mrayls) | 30.8 |
| Electrical-mechanical coupling coefficient $k_{33}$ | 0.70 |
| Relative permittivity $\varepsilon_{33}^T$ | 1300 |

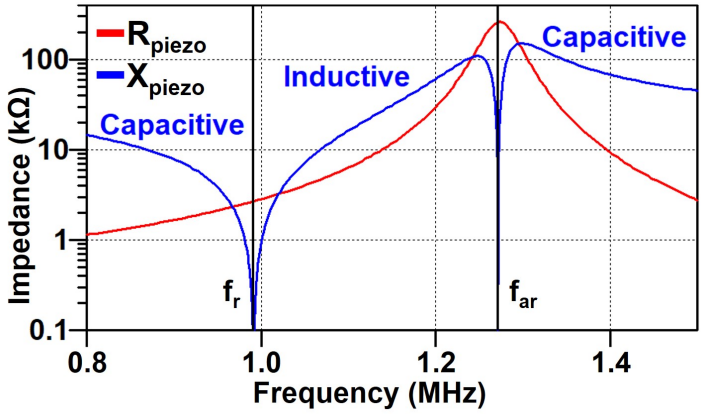


Figure 3.5: Impedance plot of the BVD model: resistive part $R_{piezo}$ and reactive part $X_{piezo}$ of the total impedance $Z_{piezo}$. The capacitive and inductive regions, and the resonance frequency ($f_r$) and anti-resonance frequency ($f_{ar}$) are indicated.

factor $0.93$. Between the resonance frequencies the reactive part is inductive, outside this band it is capacitive.

For other materials like PZT5H and $BaTiO_3$ the resonance frequencies and resistances are in the same order for the same sizes. For $LiNbO_3$ the resistances are two orders of magnitude higher, mostly because of a much lower relative permittivity. Piezo-electric transducers are often made of PZT4 and PZT5H but these contain lead, which is non-biocompatible, and therefore require a complex design. $BaTiO_3$ and $LiNbO_3$ are lead-free and could be biocompatible [21].

The peak open circuit voltage $V_{oc}$ is [25]:

$$V_{oc} = \sqrt{8 \times PCE \times I_{acou} \times A \times R_{piezo}} = \sqrt{8 \times PCE \times P_{acou} \times R_{piezo}} = \sqrt{8 \times P_{el,av} \times R_{piezo}} \quad (3.10)$$

Where the average acoustic intensity ($I_{acou}$) multiplied by the area of the transducer ($A$) and the power conversion efficiency is equal to the average available electrical power ($P_{el,av}$).

### 3.2.4. Thévenin equivalence

In literature, often, a model is simplified to a Thévenin (or Norton) equivalent circuit. The circuit is thus simplified to a black box. However, this is only valid around one frequency. Other frequency contents are not covered in the Thévenin equivalence. As an example, the BVD model has two branches with reactive components, so a Thévenin equivalent circuit is only valid around one frequency. Often a circuit produces extra frequencies next to the acoustic frequency because of, for example, a rectifier. For first insights a Thévenin equivalent circuit is good enough, but for simulations it should not be used.

## 3.3. Conclusion

The Mason and KLM modelling techniques integrate both the acoustic and electrical domains in an electrical equivalence. For our purpose this is not needed because the acoustic link has been studied a lot. Maximum acoustical power could be available at the receiver due to the high maximum acoustic intensity limit, low losses and acoustical focusing techniques. For our case the BVD model is therefore good enough for modelling the ultrasonic link. It provides insight in frequency behaviour around the resonance frequency at the receiver and is simple to implement in the electrical model of the receiver. Simplifying it into a Thévenin equivalent model is possible when there are no other frequencies than

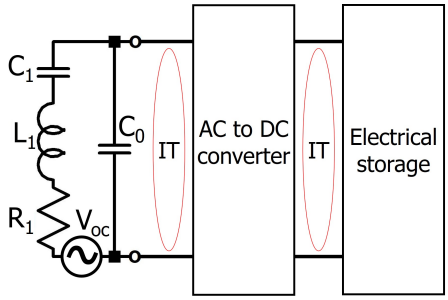


Figure 3.6: The electrical model of the receiver at ultrasonic wireless power transfer that is used from here on. The piezo-electric receiver is modelled with the BVD method and indicated are the locations that could be used for impedance transformations (IT) to achieve maximum power transfer.

the acoustic frequency involved or for first insights, but in simulation the BVD model should be used.

Figure 3.6 shows the model that is used from here on in this thesis. Impedance transformations are probably needed to achieve maximum power transfer to the storage element. These could be made both at the receiver side of the rectifier and at the storage side of the rectifier. The assumption is that there is enough available electrical power ($P_{el}$). In the next chapter we will research how we could get maximum power transfer from the piezo-electric receiver to the electrical storage element.

# 4

# Maximum power transfer method

The ultrasonic wireless power transfer link is characterized in the previous chapter. For maximum power transfer to the electrical storage element we have to think of the following question in this chapter:

***Question 3**: What methods could be employed for maximum power transfer (MPT) to the electrical storage element?*

The last figure of previous chapter (Figure 3.6) gave the basics for the ultrasonic powering system. In this chapter we will focus on the method to get maximum power transfer to the electrical storage.

First, the ideal situation for matching the piezo-electric element to the electrical storage will be outlined. Second, the power conversion system will be introduced. It is followed by the state of the art methods for maximum power transfer. The new proposed method will be designed in the next section. The conclusion will summarize this chapter and answer its question.

## 4.1. Matching piezo-electric receiver and electrical storage

For maximum power transfer, the source and load impedances of the power conversion circuit should match each other. So for a piezo-electric element as a source, the circuit hereafter (the load) should match the impedance of the transducer. In Figure 4.1 the situation is shown where the piezo-electric element is perfectly matched to a load. For maximum power transfer, $Z_{piezo} = Z^*_{load}$ is required. All waveforms in the circuit are sinusoidal.

### 4.1.1. Load matching through AC to DC conversion

However, the situation is more complex. An IMD requires a stable positive direct voltage and not the alternating voltage that is generated at the piezo-electric receiver. So the voltage should be converted to a positive voltage. As power is the product of voltage and current, the current should also always be made positive for continuous positive power into the load. For this a rectifier could be used. There

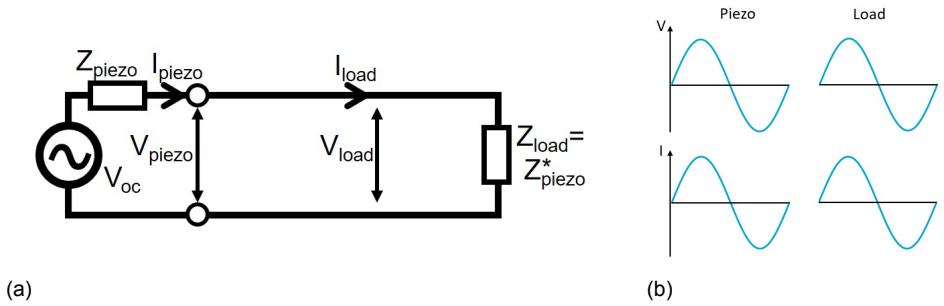


(a) (b)

Figure 4.1: (a) Matching the load to the piezo-electric element. (b) the waveforms in this circuit for purely resistive impedances.

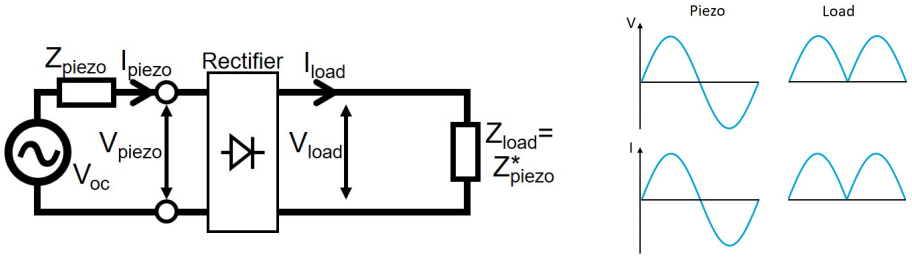


(a) (b)

Figure 4.2: (a) Matching the load through a rectifier to the piezo-electric element. (b) the waveforms in this circuit for purely resistive impedances.

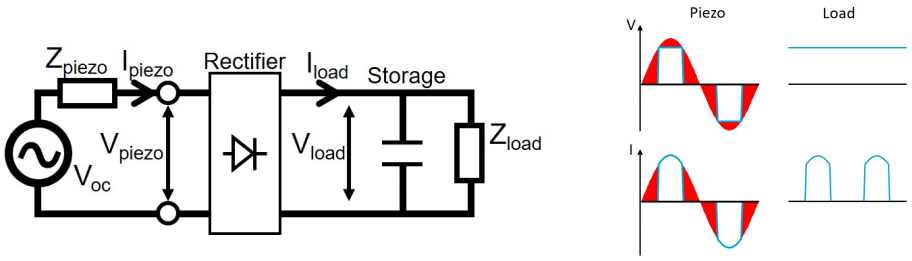


(a) (b)

Figure 4.3: (a) Adding a storage-element to 4.2 makes matching a non-linear challenge. (b) the waveforms in this circuit for a purely resistive $Z_{piezo}$, the red shaded regions indicate lost power.

are various ways of rectification but in essence the current is redirected such that the voltage and the current at the output are continuously positive. Therefore, $Z_{piezo} = Z^*_{load}$ still holds for a perfect match.

Rectification however does not make a stable direct voltage as is shown in Figure 4.2. The voltage and current waveforms at the output of the rectifier are only the absolute variants of the alternating voltage and current.

### 4.1.2. Waveform matching to a stable DC voltage

Figure 4.3 shows what the waveforms look like when a stable voltage at the IMD side is introduced, for example when a capacitive electrical storage element is used here. $Z_{load}$ is decoupled from the source by the capacitor so a match has to be made with the capacitor. At the piezo-electric source the waveform of both voltage and current are sinusoidal for maximum power transfer. At the storage capacitor the voltage is a stable DC voltage. $V_{piezo}$ should be higher than the DC voltage $V_{load}$ to open the rectifier and to let current flow in the direction of the storage element. Consequently most of the power is lost. The waveform has to be converted into a more optimal one for maximum power transfer. This conversion could also be called waveform matching instead of impedance matching because the matching should focus on the perfect waveforms.

## 4.2. System overview of power conversion

Figure 4.4 shows the general block diagram of the power conversion circuit at the receiver that follows from the analysis of the previous section. The piezo-electric receiver, the rectifier and the storage element are fixed blocks with each its functionality but in between these blocks, impedance transformations could be designed. At both the AC side and the DC side of the rectifier an impedance transformation could be designed. The two impedance transformations plus rectifier should also convert the waveform.

### 4.2.1. Piezo-electric receiver characterization

The ultrasonic piezo-electric receiver is characterized in Chapter 3. The Butterworth-Van Dyke model is used for the piezo-electric receiver. In Chapter 5 a piezo-electric receiver is chosen to compare

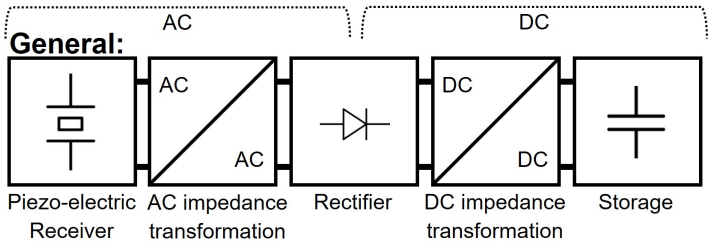


Figure 4.4: receiver power conversion block diagram.

different methods for maximum power transfer.

### 4.2.2. IMD characterization

A specific IMD is not chosen, so it could be any of many possible IMDs for different applications. As is stated in Chapter 1, the average power consumption of an IMD is in the range of some µW to some mW. We assume that it has energy storage for fluctuations both in incoming power and power demand.

### 4.2.3. Energy storage

The power demand of an IMD changes with time because of communication, electrical or optical stimulation, calculations, pumping of fluids or other high power demanding reasons. The incoming power also changes as is shown in Chapter 3. Therefore these power flows should be decoupled with an energy buffer to ensure reliable operation of the IMD. This buffer could also be bigger to enable a system that is recharged regularly via the ultrasonic powering link. The most used options for storage of the energy are in the electrical or in the electro-chemical domain.

#### Electrical domain

In the electrical domain energy could be stored in a capacitor or a supercapacitor with capacitance $C$ in farad. The energy is stored in the electric field by applying a voltage over the capacitor $V_c$, with:

$$E = \frac{1}{2} C V_c^2 \tag{4.1}$$

The voltage over the capacitor is not constant when the capacitor is charged or discharged. The capacitance is defined with:

$$C = \frac{\varepsilon A}{d} \tag{4.2}$$

With $\varepsilon$ the permittivity, $A$ the area of the capacitor plate(s) and $d$ the distance between the plates. A capacitor needs area to store the energy.

#### Electro-chemical domain

Electric energy could also be transferred to another domain to store the energy in. The electric to chemical transformation within batteries is the most used one. The voltage depends on the state of charge but is much more constant than the voltage of capacitors because of the base-voltage of a battery. A battery could be modelled with a capacitor and a resistor in series with a voltage source [26].

#### Modeling the energy storage

We choose to model the energy storage as a big capacitor at an initial voltage. The voltage is therefore constant at the initial voltage. The focus of this project is on the method to get maximum power transfer to this storage element.

### 4.2.4. Rectifier

A rectifier ideally steers the current in the right direction without introducing losses or parasitic effects. Therefore it introduces no mismatch in impedances and waveforms. In Chapter 5 a rectifier will be chosen to compare the different maximum power transfer methods.

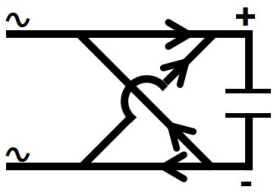


Figure 4.5: Rectifier current redirections to an electrical storage element with a DC voltage. All currents in other directions should be blocked.

The rectifier has to enable some directions for current but also to disable some, in Figure 4.5 they are shown.

A rectifier could be implemented in three different ways:

- **Passive:** A passive rectifier uses diodes to ensure single-direction current. These have a minimum forward voltage to open and thus a continuous loss of power. It is not efficient and slow because it needs its own voltage to open.
- **Active passively used:** With active elements (transistors) a gain in efficiency could be obtained. These could be used in a passive way where its controlling port (gate or base) is connected to one of the already available voltages so that the transistors open at the right moment and the current flows in the right direction.
- **Active:** Active elements could also be used in an active way by using a control signal on the controlling port (gate or base) to open the transistors. This control signal is generated in a controller. This method could be the most efficient but is also the most complex of the available methods.

As a model we use ideal rectifiers because real rectifiers could approximate ideal rectifiers and because the basic function of redirection is part of all methods.

### 4.2.5. Impedance transformations

Possible impedance transformations in the electrical domain are [27]:

- **Transformer:** an AC signal is needed to operate a transformer. The waveform and power are preserved but voltage and current are transformed. Transformers are difficult to implement on-chip.
- **Resistors:** perform a purely real impedance transformation but introduce losses.
- **Series reactance:** to obtain a transformation at the reactive part of the impedance, so a phase shift without losses is possible. Could only be used when the resistive parts of the impedances are equal and is only valid for one frequency.
- **Parallel reactance:** could be used for transformations at both the resistive and reactive part of the impedance but is also only valid for one frequency.
- **Network of reactances:** a combination of at least one series and one parallel reactance form an L-shaped network. They can make every transformation but are limited by the Q-factor of the components used. Combining multiple L-shapes gives T-shape, $\pi$-shape or more complex circuits for wider bandwidth.
- **Switched converters:** boost, buck and other types of converters also perform an impedance transformation. The boost converter is the only one with a continuous input current and could therefore be used as a matching circuit. A discontinuous switched input current, however, leads to a switched and fast varying input impedance with $Z_{in} = U/I$, so often a poor match is made.

With varying power or non-ideal components like diodes, non-linear behaviour is introduced in the circuit. Obtaining a match requires a varying impedance transformation circuit with varying transformers, capacitors, inductors or resistors. A switched converter could be used with varying duty cycle and/or varying frequency.

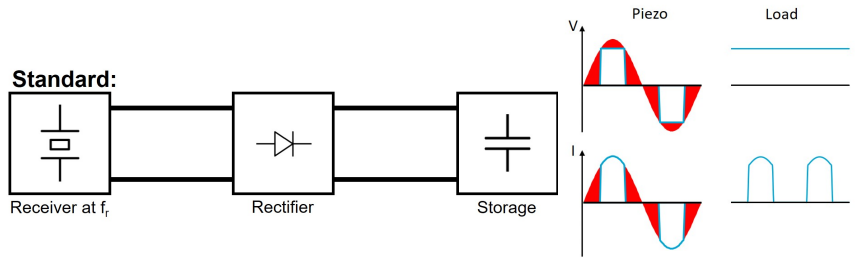


Figure 4.6: (a) Standard method without impedance transformations. (b) The waveforms in this method. The red shaded regions indicate lost power.

## 4.3. State of the art methods for maximum power transfer

For ultrasonic powering two different method for power transfer are found. First the standard method without impedance transformations will be introduced. Secondly, a method with a varying frequency is investigated.

### 4.3.1. Standard with no impedance transformations

The most used method has no impedance transformations and connects the piezo electric element to the rectifier, which is directly connected to the storage element. See Figure 4.6. It is used for example in [25]. It is easy to implement and at a certain power point it could give high efficiency. See Chapter 6.

According to Equation (3.10), the $V_{oc}$ varies with the varying $P_{acou}$, so much power is lost. In Figure 4.6 this is indicated with the red shaded regions. Two phenoma introduce losses:

1. **Voltage flattening:** Voltage peaks of $V_{piezo}$ are flattened out because it can not go higher than the DC voltage.
2. **Current blocking:** no current will flow when the voltage is too low because the rectifier only opens when $V_{piezo} > V_{load}$.

### 4.3.2. Varying frequency

In the paper of Chang et al. [21] the frequency of the acoustic waves is varied so the impedance at the receiver changes. The impedance variation as a function of frequency is shown in Figure 3.5. This method is also tested by performing an experiment with discrete components. By increasing the frequency, from $f_r$ at high $P_{acou}$ to $f_{ar}$ for low $P_{acou}$, $R_{piezo}$ increases. The peak open-circuit voltage of the piezo-electric receiver is therefore constant with Equation (3.10), solving the biggest problem of the standard method. The method is shown in Figure 4.7. Tuneable capacitor banks compensate for the varying inductive behaviour of the piezo-electric element. The current is lagging because of the inductive behaviour, but with the capacitor banks the phase is reset to zero. Communication back to the transmitter closes the control loop so the frequency and power level could be adjusted. The whole circuit could be implemented on chip. This method gives an increase in efficiency but has some disadvantages:

- For PZT4 material the PCE is highest ($\sim 1$) at $f_r$; at higher frequencies the PCE drops (to $\sim 0.5$) and the losses in tissue are higher as well.
- No storage is used, the power efficiency measurements are done behind the rectifier where a resistor models the load, so no realistic load is used.
- Since the frequency needs to be tunable, there has to be constant communication from the IMD back to the acoustic transmitter about the received power, to close the control loop. This consumes power.
- The constant communication has a delay, so during a cycle the power level and frequency could not be adjusted. Only after some time the adjustments could be done so often the impedance match is not perfect.
- The method is a non-generic solution because it only works for specific piezo-electric receivers of the right material and dimensions so the correct impedance range is available.

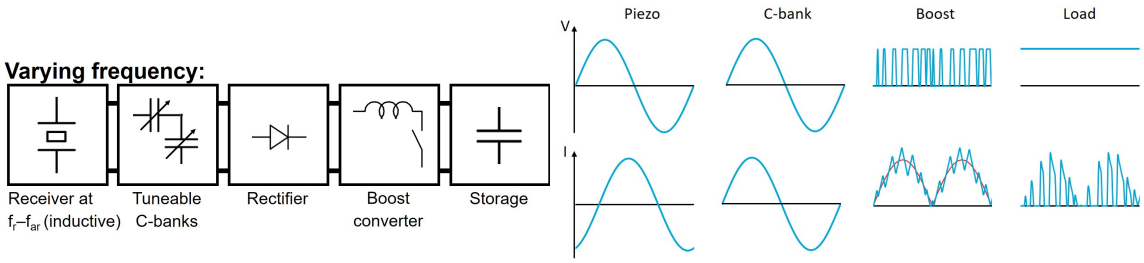


(a) (b)

Figure 4.7: (a) Varying frequency method with tunable capacitor bank and boost converter. The communication back to the acoustic transmitter is not shown. (b) The waveforms in this method.

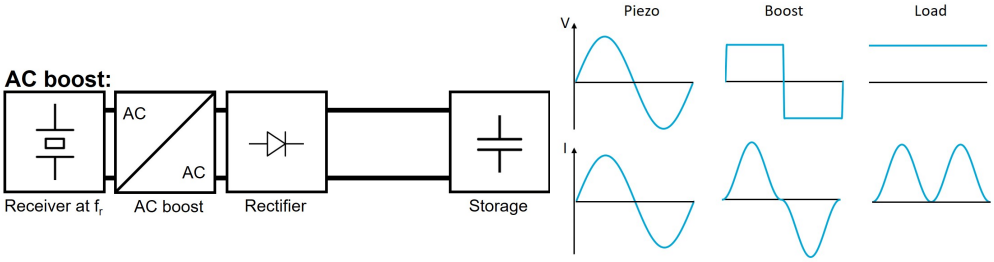


(a) (b)

Figure 4.8: (a) AC voltage boost with a continuous load current. (b) The waveforms in this method.

Since the power measured in [21] is only the rectified AC-signal, an extra DC/DC boost converter is added at the DC side of the rectifier to ensure efficiently charging the capacitor. This converter tracks the current. Both impedance transformation locations are thus utilized in this method.

## 4.4. Proposed method for maximum power transfer: AC boost

As the current methods have big disadvantages we would like to propose a new method for maximum power transfer at the receiver. This section will discuss the ideal solution and a derived method for maximum power transfer.

### 4.4.1. Boost the AC voltage and current

To ensure all power will overcome the voltage barrier of the rectifier and storage it has to be boosted or lowered, without losing power, see Figure 4.8. At moments the voltage is boosted, the current is not boosted so the current will be lowered by the boost factor. When the voltage is lowered, the current is boosted. This continuous voltage and current boost could be performed by a tuneable transformer which continuously changes the transformer-ratio for a continuous match. Such a device is currently not available but it could be approximated by a switched converter.

### 4.4.2. AC boost converter

This new method uses an AC boost converter at the receiver side of the rectifier, see Figure 4.9. At high switching frequencies ($f_{sw} \gg f_r$), the receiver voltage is boosted so all power can overcome the voltage barrier of the rectifier and storage. The voltage waveform in front of the rectifier is transformed into a pulse width modulated square wave. An advantage of the boost topology is the continuous input current that is required in matching, as zero current means a high impedance.

To realize the maximum power transfer theorem the following relation should be implemented by the boost converter circuit when the receiver is operating at resonance frequency:

$$I_{piezo} = V_{piezo}/R_{piezo} \tag{4.3}$$

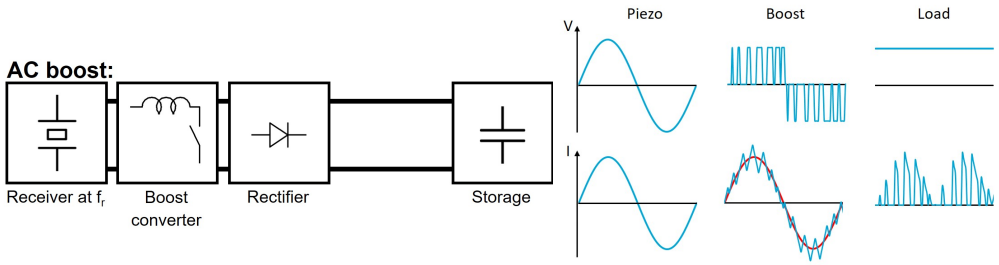


(a) (b)

Figure 4.9: (a) AC boost method. It is derived from the ideal circuit of Figure 4.8. (b) The waveforms in this method.

The current from the piezo-electric element should follow the voltage waveform, scaled down by the impedance of the piezo-electric element ($Z_{piezo}$). This impedance is real (only $R_{piezo} \neq 0$) at both resonance frequencies, which is an advantage as there is no leading or lagging current. Both current and voltage have at the same moment zero-crossings with zero power. The power from the piezo-electric element and into the storage element are always positive as both voltage and current have continuously the same sign.

The disadvantage of the boost topology is the inability to lower the voltage, it can only boost the voltage up. Therefore the voltage at the storage element should be higher than the peak $V_{piezo}$.

## 4.5. Conclusion

Three methods are presented in this chapter. Two methods are taken from the literature: the standard method and the method with varying frequency. The standard method is only efficient around one power level, the varying frequency method tries to solve it but needs two impedance transformation circuits. The newly developed method is the AC boost method and uses a boost converter at the AC side of the rectifier so only one impedance transformation circuit is needed.

In the following chapter a comparison strategy for this three methods will be developed.

# 5

# Comparison strategy for maximum power transfer methods

Two methods for maximum power transfer were taken from literature and one method is newly developed in the previous chapter. To make sure we can compare these methods we have to know the behaviour of the critical parts. In this chapter we will investigate the following question:

***Question 4**: How could the MPT methods be compared in electrical simulation?*

First a method for comparison will be developed. The design of all important elements follows. The simulation method is presented last.

## 5.1. Approach for simulation comparison of the three methods

In the paper of Chang et al. [21] the varying frequency method is presented. This method is validated with simulations and an experiment with discrete components. To be able to compare the different methods the chosen components should have comparable performance measures. As the block diagrams of Figures 4.6, 4.7 and 4.9 show, the three methods have mostly the same blocks. By using the same components per block in every method the circuits become comparable. The aim for choosing components is thus to use the same components as in [21]. The components will be designed for simulation in the following order:

1. **Piezo-electric element:** the driving source of the power conversion circuit with a certain impedance and power level.
2. **Electrical storage element:** as all the power should go here we have to design it before the impedance transformation circuits.
3. **Rectifier:** an off-the-shelf component that efficiently redirects the current.
4. **Boost converter:** consisting of an inductor, a bi-directional switch and the control of the converter. It should boost the power for maximum power transfer in both the varying frequency method and the AC boost method.

## 5.2. Design of the piezo-electric element

The piezo-electric element is the most crucial part of the power conversion circuit while it converts the acoustic power into electric power.

The piezo-electric element used in [21] has the properties as is shown in Table 5.1. The element is measured in a bath with mineral oil and it is placed on a PCB with a hole such that air backing is assured and no acoustic energy could leaks here. The measured frequencies are slightly off the calculated frequencies with the BVD model, therefore the correction factor is set to 0.93 in their research. The calculated $R_1$ is close to the measured $R_r$. It is about $15\%$ off. It should be approximately the same. The

Table 5.1: Properties of the constructed piezo-electric element of [21] and BVD circuit parameters calculated with these properties.

| Property | Value |
|---|---|
| Material | PZT4 |
| $f_r$ Measured (MHz) | 0.96 |
| $f_{ar}$ Measured (MHz) | 1.27 |
| $R_r$ Measured (kΩ) | 2.28 |
| $R_{ar}$ Measured (kΩ) | 158 |
| $W$,$L$ (mm) | 1.1 |
| $t$ (mm) | 1.5 |
| $Z_F$ Mineral oil (MRayls) used in measurement | 1.16 |
| $Z_F$ Soft tissue (MRayls) | 1.5 |
| $Z_B$ Air (Rayls) | 400 |
| BVD correction factor | 0.93 |
| BVD $R_1$ (kΩ) | 2.66 |
| BVD $C_0$ (pF) | 4.73 |
| BVD $C_1$ (pF) | 3.12 |
| BVD $L_1$ (mH) | 8.30 |
| BVD $f_r$ (MHz) | 0.99 |
| BVD $f_{ar}$ (MHz) | 1.27 |

difference could come from measurement uncertainties or modelling inaccuracy. Figure 3.3 shows the power conversion efficiency and the measured and calculated resistance as a function of the frequency of this piezo-electric element. The maximum acoustic power at the front area is:

$$P_{acou,max} = P_{limit} \times W \times L = 7.2 \text{ mW/mm}^2 \times (1.1 \text{ mm})^2 = 8.71 \text{ mW} \tag{5.1}$$

In this method, $R_{piezo}$ is changed with the varying frequency to match to the input resistance of the conversion system. For lower $P_{el,av}$, $R_{piezo}$ is therefore higher and their product remains the same. $V_{oc}$ is therefore held constant as Equation (3.10) shows.

### Usability in the three methods

In the varying frequency method, the resistance of the piezo-electric element varies so as to match it to the power conversion circuit. In the other methods this is not the case. In the standard method, the resistance of the piezo-electric element should be close to the expected resistance of the circuit for optimal power transfer. This is only true around one power level. The circuit has no constant input resistance as it varies with the available power:

$$R_{circuit} = \frac{V_{piezo}^2}{2P_{circuit}} \tag{5.2}$$

For maximum power transfer $V_{piezo}$ should equal $1/2 V_{oc}$ for $R_{circuit} = R_{piezo}$. In Figure 5.1 $V_{oc}$ is plotted for different $R_{piezo}$ as a function of $P_{el,av}$. For the piezo-electric element at resonance frequency the resistance is $2.28$ kΩ. So for maximum power transfer at maximum $P_{el,av} = 8.71$ mW, $V_{piezo}$ is $6.10$ V. At $1$ mW it is only $2.14$ V. As the piezo-electric element produces high enough voltages at the maximum power level, down to about $1$ mW, we can conclude that this piezo-electric receiver is good for the standard method.

In the AC boost method, the AC boost converter should make a continuous resistive match. For efficient operation the boost factor should be low. A boost converter can only increase the voltage so the $V_{oc}$ should be low enough to enable boosting over a wide power range. As can be seen in Figure 5.1 the piezo-electric element of [21] seems good for this purpose. From about 2 mW $V_{piezo}$ can part of the time not be boosted anymore, because of the high peak $V_{piezo}$

### Model

The BVD model will be used with the parameters from Table 5.1.

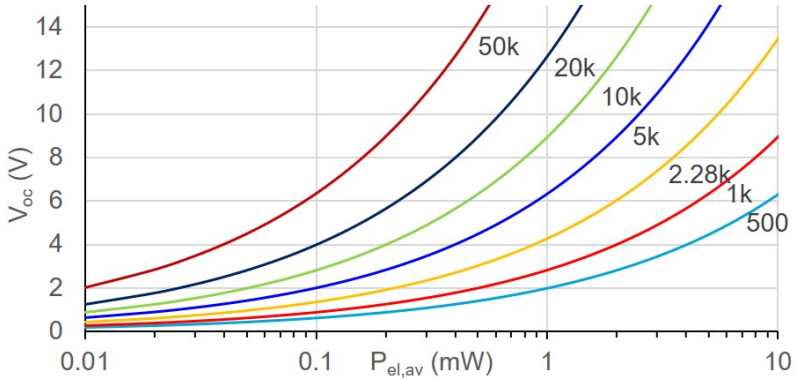


Figure 5.1: $V_{oc}$ for different $R_{piezo}$ as a function of $P_{el,av}$.

Table 5.2: Properties of the diodes HSMS-282X used in [21], datasheet: [30].

| Property | Value |
|---|---|
| Minimum breakdown voltage $V_{BR}$ (V) | 15 |
| Maximum forward voltage $V_F$ (V) @ $I_F$ (mA) | 0.34 @ 1 |
| Maximum forward voltage $V_F$ (V) @ $I_F$ (mA) | 0.5 @ 10 |
| Maximum reverse leakage $I_R$ (nA) @ $V_R$ (V) | 100 @ 1 |
| Maximum capacitance $C_T$ (pF) | 1.0 |
| Typical dynamic resistance $R_D$ (Ω) | 12 |

## 5.3. Design of the storage element

A storage element is needed for fluctuations both in received and used power. As [21] is not using a storage element we have to add this to this method. Both batteries and capacitors are possible in simulation. We choose to use a big capacitor with a constant voltage so research about the power flow could be done.

### Real components

For a future implementation, the storage element should be small enough to fit in a tiny IMD. With current technology, supercapacitors can store up to $30\,\mu Wh/mm^3$ [28], and rechargeable batteries up to $350\,\mu Wh/mm^3$ [29]. IMDs have an average power consumption in the range of µWs to some mWs [5]. In devices that have a power demand of mWs with a capacitor of $1$ mm$^3$, the storage element could provide power for about $1$ minute. In µWs power demanding devices with a battery of $5$ mm$^3$, the storage element could provide power for about $1$ month. Depending on the application the right storage element could be chosen, but in every case it could at least store the average electrical power for $1$ minute.

### Model

A $1$ F capacitor is used in simulation at an initial condition of $2$ V as this is well above the transistor threshold voltage and within the specifications of current IMDs and IC technology.

## 5.4. Design of the rectifier

The rectifier should efficiently redirect the current so all energy could be stored in the storage element.

The rectifier used in [21] is a bridge configuration of the surface mount RF Schottky barrier diodes HSMS-282x [30]. These diodes are well documented and simulation parameters are give in the datasheet, these are listed in Table 5.2.

### Usability in the three methods

As the specifications of this rectifier are among the best in the field of surface mount rectifiers, this rectifier should be used for comparison in all three methods. A remark has to be made for the AC boost method, the frequency at which the rectifier is turned on and off is much higher so the losses are

Table 5.3: SPICE modeling parameters of the HSMS-282x diodes [30].

| Parameter | Value |
|---|---|
| $B_V$ (V) | 15 |
| $C_{J0}$ (pF) | 0.7 |
| $E_G$ (eV) | 0.69 |
| $I_{BV}$ (A) | 1e-4 |
| $I_S$ (A) | 2.2e-8 |
| $N$ | 1.08 |
| $R_S$ (Ω) | 6.0 |
| $P_B$ or $V_J$ (V) | 0.65 |
| $P_T$ or $X_{ti}$ | 2 |
| M | 0.5 |

also higher. A different structure with active transistors would make a big difference in terms of rectifier efficiency.

### Model

The SPICE modeling parameters of the rectifier diodes are presented in Table 5.3. These are used for the diodes in a full-wave bridge configuration.

## 5.5. Design of the control of the boost converter

In this section, the control of the boost converter will be designed. In [21] the control of the capacitor bank is not designed and per power level a different discrete capacitor is soldered in the circuit. For the boost converter, there is control needed because the method is based on a controlled switch. This control however will not be implemented in a hardware design, as it could be a project on its own.

### Current tracker

In the ideal situation the controller ensures that the current is tracking the voltage curve perfectly with:

$$I_{piezo} = V_{piezo}/R_{piezo} \tag{5.3}$$

This holds for both the AC boost converter method and the varying frequency method with a DC boost converter. However, the current is fluctuating because of the switching. The current first increases when the switch is closed and energy is stored in the inductor. After some time the switch is opened and the inductor is boosting the voltage, resulting in a decreasing current.

The switching frequency $f_{sw}$ of the boost converter should be higher than the frequency of the acoustic signal. The acoustic frequency is about 1MHz, $f_{sw}$ should be at least one order higher, so more than 10MHz.

### Control method possibilities

Different control methods are possible to achieve that the current tracks the voltage curve. The possible methods for determining the switching moments are:

- **Energy based switching:** the energy stored in the inductor is more than enough to overcome the storage plus rectifier barrier, so the switch opens. When the energy stored in the inductor is decreased enough, the switch closes again. Both the energy stored in the inductor and the energy needed for effective boosting should be estimated.
- **Time based switching:** after a certain amount of time, the switch opens and closes. These timings could be programmed into the controller for different power levels.
- **Threshold based switching:** based on a high and low threshold for the current the switch opens and closes. Only the current and voltage have to be measured for this method and it could be implemented with a comparator for each threshold.

These methods could be combined with the following two principles that both have their own impact on efficiency:

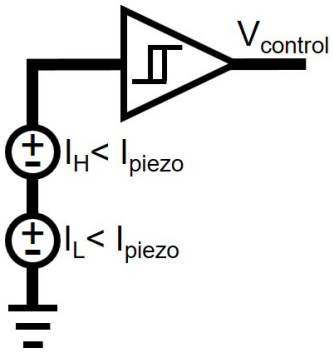


Figure 5.2: The structure of the control. Two comparators in series produce a voltage. Only when both are off or both are on the Schmitt trigger will change state.

- **Non-zero current switching:** the current tracks the ideal curve closely, so there is always a nearly perfect impedance match.
- **Zero current switching:** the switching is much more efficient and the average current provides a good impedance match. However, the actual current is most of the time far away from a perfect impedance match.

As the proposed new method is about tracking the ideal current curve as closely as possible we decide to implement non-zero current threshold based switching.

### Model

The control is implemented by using two comparators and a Schmitt trigger as is shown in Figure 5.2. $I_H$ and $I_L$ are defined as follows:

$$I_H = a_h \times V_{piezo}/R_{piezo} \tag{5.4}$$

$$I_L = a_l \times V_{piezo}/R_{piezo} \tag{5.5}$$

$$\tag{5.6}$$

Where $a_h$ is the upper threshold factor which is always more than 1, and $a_l$ is the lower threshold factor which is always less than 1. At every power level the threshold factors have to be adjusted for optimization of power transfer. The possible power consumption of this control is not taken into account as this requires an extensive design.

## 5.6. Design of the boost inductor

As the inductor of the boost converter is difficult to implement on chip, the discrete component inductor should be small enough to fit in the small IMD. It should have enough inductance to store the energy. Part of the time it stores energy, the other part it delivers energy by boosting the voltage. The energy delivered by the inductor, from the time $t_h$ when the current is too high ($I_h$) and the switch goes off, to the time $t_l$ when the current is too low ($I_l$) and the switch goes back on, is:

$$E_{L,del} = \int_{t_h}^{t_l} P_{L,del}(t)dt = \int_{t_h}^{t_l} \Big(V_{boost}(t) - V_{piezo}(t)\Big) I_{piezo}(t)dt \tag{5.7}$$

The slope of $I_{piezo}$ during charge and discharge of the inductor should be as steep as the slope of $I_{ideal}$ at its maximum to ensure it is able to follow the ideal curve. The maximum slope is around zero-crossings of the sinusoidal current:

$$\text{slope}_{max} = \left(\frac{dI_{piezo}(t)}{dt}\right)_{max} = \omega \times I_{piezo,max} \tag{5.8}$$

The maximum $P_{el,av,max} = 8.712$ mW with $V_{piezo,max} = 7.29$ V, gives $I_{piezo,max} = 1.195$ mA. So $\text{slope}_{max} = 2\pi \times 1\text{MHz} \times 1.195\text{mA} = 7.51$ kA/s. The maximum voltage boost provided by the inductor is when $V_{piezo}$ is around 0 V as well, so $V_{L,max} = V_{boost,max}$. Further, $V_{boost,max} = 2.68$ V as

Table 5.4: Level 1 SPICE model for NMOS devices in 500nm technology of [32].

| Parameter | Value | Parameter | Value |
|---|---|---|---|
| LEVEL | 1 | Gamma | 0.45 |
| NSUB | 9e+14 | UO | 350 |
| TOX | 9e-9 | CJ | 0.56e-3 |
| MJ | 0.45 | CGDO | 0.4e-9 |
| VTO | 0.7 | PHI | 0.9 |
| LD | 0.08e-6 | LAMBDA | 0.1 |
| PB | 0.9 | CJSW | 0.35e-11 |
| MJSW | 0.2 | JS | 1.0e-8 |

$V_{storage} = 2$ V plus two times a forward voltage of the rectifier of $2V_F = 0.68$ V. So for the case when all parameters are assumed to be maximum, the inductor should be smaller than:

$$L_{max} = \frac{V_{L,max}}{\text{slope}_{max}} = \frac{V_{boost,max} - V_{piezo}}{\omega \times I_{piezo,max}} = \frac{2.68\text{ V} - 0\text{ V}}{2\pi \times 1\text{ MHz} \times 1.195\text{ mA}} = 357\,\mu\text{H} \tag{5.9}$$

As this large inductance is the maximum, we have to search for a smaller one. However, the smaller the inductor is, the more often we have to switch, what costs power. Therefore, we propose a $100\,\mu$H inductor because these are available in small sizes of $2-4$ mm$^3$. The selected inductor is the Coilcraft XFL2006-104ME [31], which has an inductance of $100\,\mu$H, a typical self-resonance frequency $f_0$ of $13$ MHz, a maximum DC resistance of $12.25\ \Omega$ and a volume of $2.3$ mm$^3$.

### Model

The model used is an ideal inductor in series with the DC resistance and a capacitor $C_P$ in parallel to these to model the self-resonance frequency. The capacitor is calculated with:

$$C_P = \frac{1}{(2\pi f_0)^2 L} = 1.5\text{ pF} \tag{5.10}$$

## 5.7. Design of the boost switch

For the AC boost method the switch has to be bi-directional, meaning that it should be able to let the current flow and stop in both directions. A MOSFET is a bi-directional device, and for an NMOS the source is defined as the terminal with the lowest potential. Special precautions have to be taken for on-chip design. The bulk should be connected to a source with lower potential than the source potential, blocking the pn-junction between bulk and source.

Available discrete components are all too big for usage as this boost switch. The power needed to turn the transistor on and off is too large. Therefore a model of an IC process should be used. As the goal is to enable a tiny power conversion system an IC implementation is expected. The IC technology that will be used should have all circuit voltages in its allowed range. The voltages are up to $5$ V. For example, in a $180$ nm technology, special high voltage devices are needed to work up to $5$ V.

### Model and size

In the book of Razavi on Analog CMOS design [32] a level 1 model for NMOS and PMOS devices in $500$ nm technology is presented. The $500$ nm technology can use normal devices up to $5$ V. The typical values for the level 1 parameters of the NMOS model are in Table 5.4. We will use this model with two transistors in anti-series, back-to-back. The gate voltage $V_G$ is assumed to be $2$ V, as this is the same voltage of the storage element.

Each transistor is composed of three parallel transistors, sized $500$ nm $\times\ 20\,\mu$m. These sizes follow from first order calculations:

$$C_G = n \times W \times L \times C_{ox} = n \times W \times L \times \varepsilon_0 \times \varepsilon_r / t_{ox} \tag{5.11}$$

$$= 3 \times 20e^{-6} \times 500e^{-9} \times 8.85\text{e}^{-12} \times 3.9/9\text{e}^{-9} = 0.115\,\text{pF} \tag{5.12}$$

$$P_G = f_{sw} \times \tfrac{1}{2} \times C_G \times V_G^2 = 10e^6 \times \tfrac{1}{2} \times 0.115e^{-12} \times 2^2 = 2.30\,\mu\text{W} \tag{5.13}$$

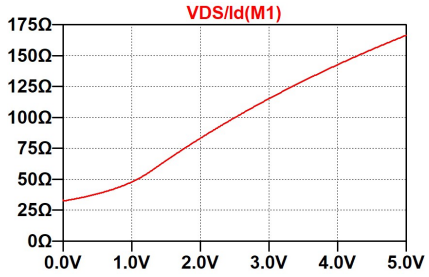


Figure 5.3: The simulated $R_{on}$ of a transistor for $V_G = 2$ V, designed in the $500$ nm technology of [32].

Table 5.5: SPICE modeling parameters [33]. Cshunt is only used when no convergence was found.

| Parameter | Value |
|---|---|
| LTspice version | XVII 2019 |
| Gmin | 1e-10 |
| Abstol | 1e-10 |
| Reltol | 0.001 |
| Chgtol | 1e-14 |
| Trtol | 1 |
| Volttol | 1e-6 |
| Sstol | 0.001 |
| MinDeltaGmin | 0.0001 |
| Cshunt | 1e-15 |
| Compression | off |

Where the gate power loss per transistor $P_G$ is insignificant at high power levels but at low power levels it will become the major loss.

Figure 5.3 shows the $R_{on}$ as a function of $V_{DS}$ for $V_G = 2$ V. As a switch it always operates at low $V_{DS}$ so the $R_{on}$ is about $30\ \Omega$. As there are two switches in anti-series the total resistance is double the $R_{on}$. This total resistance is about $2\%$ of $R_{piezo}$, so when the switch is closed the losses in the switches will be limited to $2\%$.

## 5.8. Simulation method

For simulation of the three methods LTspice [33] is used. In Table 5.5 all parameters used are listed. The methods are simulated with the components which are presented in this chapter. The allowed current range thresholds are optimized for maximum power transfer for both the varying frequency method and the AC boost method. The gate power $G_P$ is subtracted from the efficiency results. However, the varying frequency method simulations need some extra explanation.

### Varying frequency method

For the varying frequency method the components at the AC-side, i.e. the piezo-electric element, the tuneable capacitor bank and the rectifier, are not simulated but the efficiency results are taken from [21]. These efficiency results are multiplied with the boost converter efficiency for every power level. An ideal blocking diode is added to the boost converter in the varying frequency method because no rectifier follows the boost converter. The extra losses of the continuous communication for frequency adjustment and control of the capacitor banks in the varying frequency method are not taken into account, and zero communication delay is assumed, so a match is made without delay.

## 5.9. Conclusion

In this chapter, a comparison strategy is developed for the three maximum power transfer methods. The same components as used in [21] will be used in simulation and some components are designed because they were not used in there.

The same piezo-electric element fits for all three methods, its maximum available average electric power is $P_{el,av} = 8.71$ mW. For the storage element, it is shown that even the smallest element of $1$

$mm^3$ could store enough power to power a high power consuming device for $1$ minute. For the three methods, it is chosen to be a big capacitor at an initial voltage of $2$ V. The same rectifier as is used in [21], will be used in our simulation because of the outstanding specifications and well documented simulation parameters. The boost converter is designed to follow the ideal current curve closely with the non-zero current threshold based switching method. The boost inductor is chosen to be $100\,\mu H$. The boost switch is designed in a $500$ nm technology and is composed of two transistors in anti-series, each consisting of three parallel transistors of $500$ nm $\times$ $20\,\mu m$.

The simulations will be done in LTspice XVII and the results from [21] will be used in the varying frequency method.

The comparison strategy is applied and the results are presented in the following chapter.

# 6

# Simulation results maximum power transfer methods

In this chapter the three presented methods for maximum power transfer will be evaluated with the strategy of previous chapter. The question to be answered in this chapter is:

***Question 5**: What are the results of the comparison of the MPT methods?*

As the goal is maximum power transfer to the storage element, the most important result is presented first: the power efficiency comparison between the three methods. After this the results per method are presented.

## 6.1. Efficiency comparison

Figure 6.1 shows the simulation results of the power efficiency of the three methods. $\eta_{total}$ is the total efficiency from the piezo electric receiver to the storage element and $P_{load}$ is the total power into the storage element. The AC boost method is for the full power range the most efficient method, around $P_{load} = 1$ mW the efficiency is $74\%$ and this drops to $22\%$ at $P_{load} = 0.01$ mW. At $P_{load} = 2$ mW, the standard method is also $74\%$ efficient but for different power levels the efficiency is much lower, at $P_{load} = 0.1$ mW the efficiency has already dropped to $23\%$. The varying frequency method is as efficient as the AC boost method from $P_{load} = 0.01$ mW to $P_{load} = 0.1$ mW, but for higher power levels the efficiency is lower than the AC boost method.

At high power levels the efficiency of the AC boost method follows the standard method's efficiency because $V_{piezo}$ is most of the time higher than the required voltage, so no boosting happens. The method therefore acts the same as the standard method.

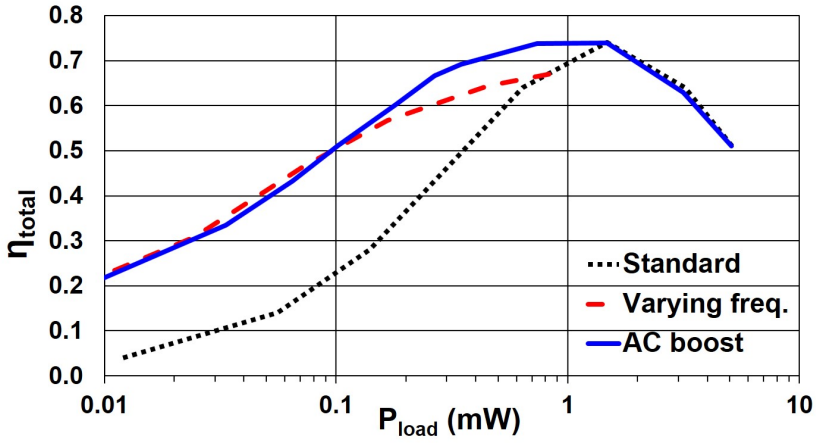


Figure 6.1: Simulation results of the power efficiency as a function of load power for the three methods.

Table 6.1: Results generated of the standard method.

| $P_{el,av}$ (mW) | $V_{oc}$ (V) | $\eta_{total}$ | $P_{load}$ (mW) |
|---|---|---|---|
| 0.2 | 2.0632 | 0 | 0 |
| 0.3 | 2.5269 | 0.04 | 0.012 |
| 0.4 | 2.9179 | 0.14 | 0.056 |
| 0.5 | 3.2623 | 0.28 | 0.14 |
| 1 | 4.6135 | 0.64 | 0.64 |
| 2 | 6.5245 | 0.74 | 1.48 |
| 5 | 10.3162 | 0.64 | 3.2 |
| 10 | 14.5893 | 0.51 | 5.1 |

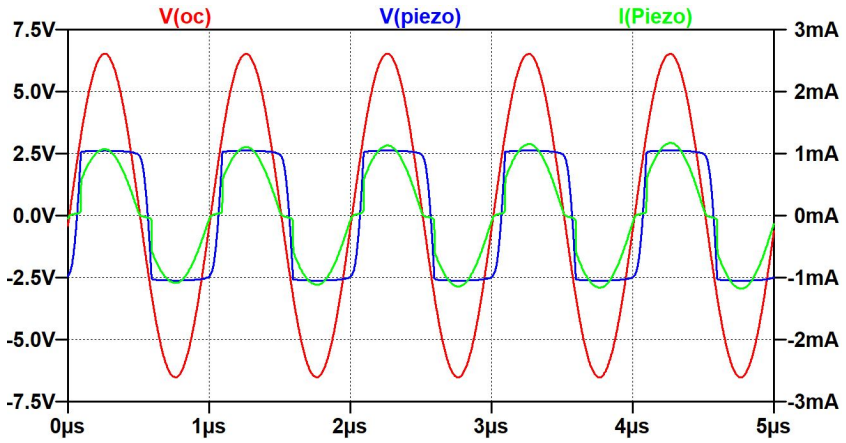


Figure 6.2: Waveforms of the simulation of the standard method at $P_{el,av} = 2$ mW.

At low power levels the AC boost method follows the varying frequency method. The gate losses $P_G$ become here the major losses so this holds for both methods.

## 6.2. Results standard method

In Table 6.1 the results of the simulation of the standard method are summarized. For every $P_{el,av}$ The peak efficiency of $74\%$ is around $2$ mW because at this power level the match with the piezo-electric element impedance is good. The rectifier is responsible for the majority of the losses at this point. The minority of losses is because of the block waveform that is made from the sinusoidal voltage waveform. Power levels above and below $2$ mW provide a less good match and therefore a much lower efficiency.

In Figure 6.2 the waveforms of the maximum $V_{oc}$, $V_{piezo}$ and $I_{piezo}$ are shown for $P_{el,av} = 2$ mW. $V_{piezo}$ is flattened and $I_{piezo}$ is part of the time zero, so power is lost. However, the flattening is less dominant as expected, because $C_0$ buffers the voltage. This could also be seen in the lagging of $V_{piezo}$ with respect to $V_{oc}$.

## 6.3. Results varying frequency method

The size of Table 6.2, with all important parameters in the efficiency of the varying frequency method, indicates the complexity of this method. The frequency $f$ and $R_{piezo}$ are read from the figures in [21], together with the efficiency result $\eta_{tune}$ at electrical power $P_{tune}$. $P_{el,av}$ is calculated with $P_{tune}/\eta_{tune}$. At low $P_{el,av}$, the boost switch gate power $P_G$ is relatively big so the efficiency of the boost converter $\eta_{boost}$ and the output power of the boost converter $P_{boost}$ decrease. The thresholds could be kept mostly constant because of the constant $V_{oc}$.

Table 6.2: Results generated of the varying frequency method. $\eta_{boost}$ is the result without the losses of $P_{gate}$. The thresholds are manually optimized. $f$, $R_{piezo}$, $\eta_{tune}$ and $P_{tune}$ values are taken from [21].

| $P_{el,av}$ (mW) | $V_{oc}$ (V) | $f$ (MHz) | $R_{piezo}$ (Ω) | $\eta_{sw}$ | $P_{gate}$ (mW) | Thres-holds | $P_{boost}$ (mW) | $\eta_{boost}$ | $\eta_{tune}$ | $P_{tune}$ (mW) | $\eta_{total}$ | $P_{load}$ (mW) |
|---|---|---|---|---|---|---|---|---|---|---|---|---|
| 0.025 | 4 | 1.26 | 200k | 0.62 | 0.0211 | 0.01-1.5 | -0.015 | 0 | 0.4 | 0.01 | 0 | 0 |
| 0.038 | 4 | 1.25 | 100k | 0.72 | 0.0131 | 0.01-1.5 | 0.0013 | 0.065 | 0.53 | 0.02 | 0.0345 | 0.0013 |
| 0.079 | 4 | 1.24 | 40k | 0.73 | 0.012 | 0.01-2.0 | 0.0245 | 0.490 | 0.63 | 0.05 | 0.3087 | 0.0244 |
| 0.154 | 4 | 1.22 | 20k | 0.82 | 0.0109 | 0.01-2.3 | 0.0711 | 0.711 | 0.65 | 0.1 | 0.4622 | 0.0711 |
| 0.294 | 4 | 1.19 | 10k | 0.88 | 0.009 | 0.01-2.5 | 0.167 | 0.835 | 0.68 | 0.2 | 0.5678 | 0.167 |
| 0.704 | 4 | 1.14 | 4k | 0.92 | 0.0068 | 0.01-2.5 | 0.4532 | 0.906 | 0.71 | 0.5 | 0.6433 | 0.453 |
| 1.37 | 4 | 1.08 | 2k | 0.93 | 0.0059 | 0.01-2.5 | 0.924 | 0.924 | 0.73 | 1 | 0.6745 | 0.924 |

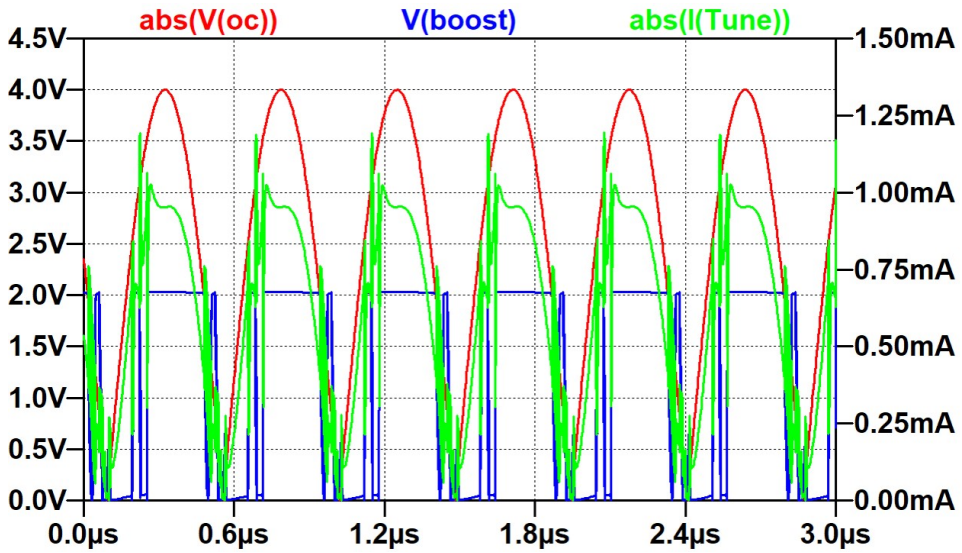


Figure 6.3: Waveforms of the simulation of the varying frequency method at $P_{el,av} = 1.37$ mW.

The following relations are applicable to the results:

$$\eta_{boost} = \frac{P_{boost}}{P_{tune}} = \eta_{sw} - \frac{P_G}{P_{tune}} \tag{6.1}$$

$$P_{load} = \eta_{boost} \times P_{tune} = \eta_{boost} \times \eta_{tune} \times P_{el,av} = \eta_{total} \times P_{el,av} \tag{6.2}$$

The $|V_{oc}|$, $V_{boost}$ and $|I_{tune}|$ waveforms of the varying frequency method are plotted in Figure 6.3 for $P_{el,av} = 1.37$ mW. Because $P_{el,av}$ is calculated of other values it is not set at 2 mW. Because of the constant $V_{oc}$ of 4 V, the voltage does not have to be boosted much. $I_{tune}$ shows steep current spikes because of the non-ideal inductor that also has a capacitive effect. Every time the voltage is switched this causes a high current for a very short time.

## 6.4. Results AC boost method

As Table 6.3 displays, the optimized thresholds are much less constant than at the varying frequency method. The efficiency peak of 74% is as high as at the standard method but the peak is wider. The efficiency is the boost result minus $P_{gate}$. Simulations are done for more power levels than for the other two methods because the trend was more difficult to find.

The waveforms of $V_{oc}$, $V_{boost}$ and $I_{piezo}$ are plotted in Figure 6.4. The voltage boosting of the boost converter is clearly visible. The current here is also showing short steep peaks because of the non-ideal inductor and the simplified transistor model. However, the normal values of $I_{piezo}$ follow the ideal sinusoidal curve closely.

Table 6.3: Results of the AC boost method. $\eta_{boost}$ is the result without the losses of $P_{gate}$. The thresholds are manually optimized.

| $P_{el,av}$ (mW) | $V_{oc}$ (V) | $\eta_{sw}$ | $P_{gate}$ (mW) | Thresholds | $\eta_{total}$ | $P_{load}$ (mW) |
|---|---|---|---|---|---|---|
| 0.02 | 0.6525 | 0.03 | 0.0060 | 0.01-9 | -0.27 | 0 |
| 0.05 | 1.0315 | 0.14 | 0.0056 | 0.01-8 | 0.028 | 0.0014 |
| 0.1 | 1.4589 | 0.39 | 0.0056 | 0.01-2.5 | 0.334 | 0.0334 |
| 0.15 | 1.7229 | 0.47 | 0.0056 | 0.01-2.3 | 0.4327 | 0.0649 |
| 0.2 | 2.063 | 0.54 | 0.0057 | 0.01-2.1 | 0.5115 | 0.1023 |
| 0.3 | 2.5266 | 0.62 | 0.0055 | 0.01-4.9 | 0.6017 | 0.1805 |
| 0.4 | 2.9175 | 0.68 | 0.0055 | 0.01-5 | 0.6663 | 0.2665 |
| 0.5 | 3.2618 | 0.7 | 0.0044 | 0.01-2 | 0.6912 | 0.3456 |
| 1 | 4.6129 | 0.74 | 0.0026 | 0.01-6 | 0.7374 | 0.7374 |
| 2 | 6.5237 | 0.74 | 0.0016 | 0.01-2.2 | 0.7392 | 1.4784 |
| 5 | 10.3148 | 0.63 | 0.0020 | 0.01-2.2 | 0.6296 | 3.148 |
| 10 | 14.5874 | 0.51 | 0.0020 | 0.3-0.6 | 0.5098 | 5.098 |

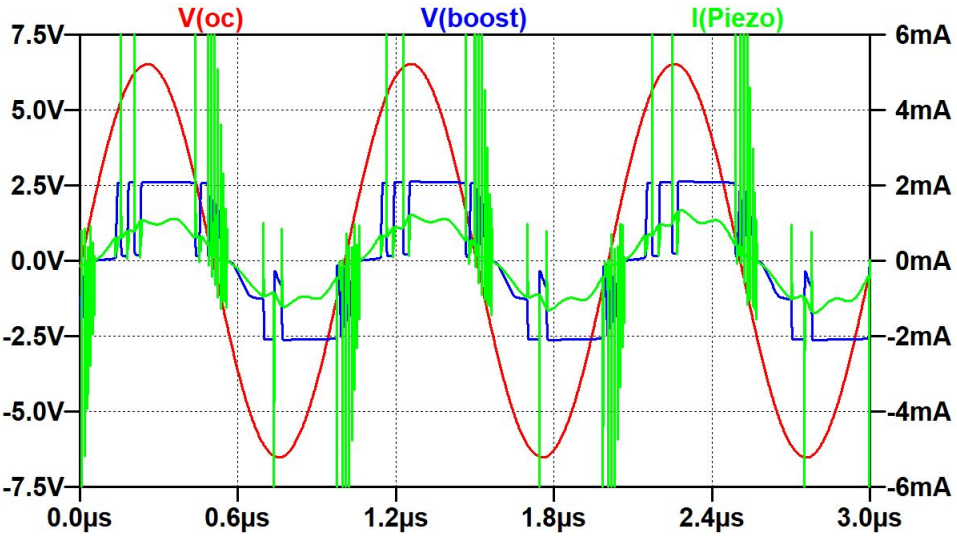


Figure 6.4: Waveforms of the simulation of the AC boost method at $P_{el,av} = 2$ mW.

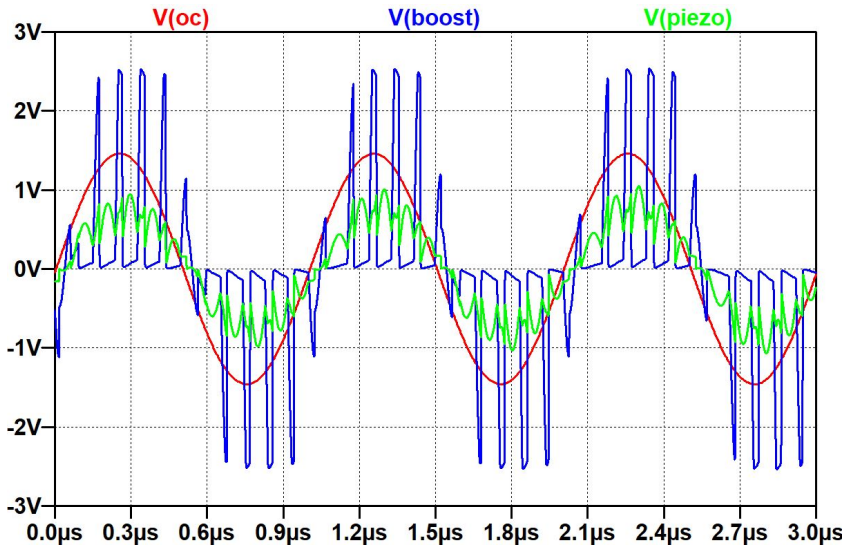


Figure 6.5: Waveforms of the simulation of the AC boost method at $P_{el,av} = 0.1$ mW.

### Control scheme

The control operates the switch when $I_{piezo}$ crosses the thresholds, but, as can be seen in Figure 6.5, the boost is sometimes to a too low voltage. So the power is not going through the rectifier but is lost. This simulation is done at low power: $P_{el,av} = 0.1$ mW with $V_{oc} = 1.4589$ V. $V_{piezo}$ is continuously about $^1/_2V_{oc}$, as is required for a perfect match.

As could be seen from the threshold values in Tables 6.2 and 6.3 the range is often not close to the ideal curve. This is because the thresholds are manually optimized and are not designed to be changed during a simulation. So for multiple full cycles the thresholds stay the same.

## 6.5. Conclusion

In this chapter, the results of the comparison are presented. The AC boost method is the most efficient power conversion method with a peak efficiency of $74\%$ at $P_{load} = 2$ mW and $22\%$ at $P_{load} = 10\,\mu$W load power. The standard method has only a small high efficiency peak around $2$ mW. The varying frequency method is as efficient as the AC boost method but the peak is lower.

The AC boost method matches correctly so the power extracted from the piezo-electric element is maximal. The boost converter uses an inductor that is non-ideal; it causes current spikes at switching moments. The boost converter does not always boost the voltage high enough because the control does not estimate the energy stored in the inductor and the energy required for efficient boosting.

A discussion of this results and the methodology used is in the following chapter.

# 7

# Discussion

In this discussion we will look back on the methodology used and the results presented in Chapter 6. We will also look forward to a potential full IC design. The focus will be on the following question:

***Question 6**: What is the validity of the approach and of the results, what are its limitations, and how could the AC boost method be utilized?*

First, the validity of the approach will be investigated. Secondly, the results presented are discussed. Next, the challenges towards a full design for the AC boost method in an integrated circuit follow. The conclusion reviews this chapter's question.

## 7.1. Validity of approach

For this project, first the AC boost method was developed that promises maximum power transfer from an AC source to a DC storage element, when ideal components are used. It results in a continuous squared sinusoidal current curve and a theoretical $100\%$ efficiency. This reasoning is straight forward and valid. From this ideal situation a practical method is developed with an AC boost converter. Here, $I_{piezo}$ tracks the ideal curve, but it is not always the perfect curve. It leads to an always close to perfect match. If this project would be repeated, the same theoretical result will follow.

Secondly, comparable circuits were designed and compared through simulation. The AC-boost method is the most efficient method for a wide power range. The simulations were done in LTspice with models of real components and the results and parameters are documented in this thesis. The circuits presented in this project were designed to be minimal and comparable with each other. This was done by using as much as possible the same components for each method, and not taking into account all losses involved in the varying frequency method. A future project would deliver the same results if similar comparable circuits would be simulated.

For the varying frequency method a $2$ V storage has a good effect on the efficiency. It is exactly half of $V_{oc} = 4$ V. Therefore, high efficiency is always possible. At low $P_{el,av}$, the boost converter consumes more power than it helps increasing the load power at this method because of the good $V_{oc}$. When a higher storage voltage has been chosen, the efficiency would have been lower. The extra diode, used in the DC boost converter of the varying frequency method, also boosts the efficiency results because of its ideality. However, even with this favored position, the varying frequency method performs less good than the AC boost method. This makes the global result, where the AC boost method is the most efficient one, even more realistic.

## 7.2. Discussion of results

The AC boost method is the most efficient method for a wide power range. It matches the piezo-electric element with the circuit following it, as expected. Maximum power is delivered by the piezo-electric element. However, the method development gave rise to higher expectations. The power loss at low power is the most important factor for lower results at low power. The biggest power losses are:

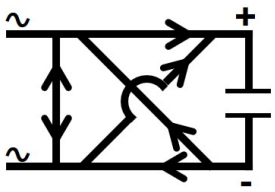


Figure 7.1: Part of the AC boost method circuit with the rectifier and the boost switch. The current directions that have to be enabled are shown with arrows, the opposite directions have to be blocked.

- **Imperfect boost converter:** The boost converter introduces high losses because of the relatively large amount of power needed at low power to switch the switch. The control is also imperfect because the threshold switching algorithm does not take into account the energy that is needed to overcome the barrier.
- **Rectifier configuration:** The rectifier is composed of Schottky diodes. These diodes introduce a loss because each diode has a forward voltage. The diodes are switched at high frequency so the parasitic capacitances are often charged and discharged, and power is lost.

Potential solutions to these losses will be presented hereafter, in Section 7.4.

## 7.3. Limitations

As the developed method is validated with simulations of minimal circuit designs there are limitations involved in the study. Not all aspects of a full design could be simulated. For example, the influence of the pads of an IC are not yet investigated. The results of the AC boost method and the varying frequency method are close together at low power. A more extensive study is needed to estimate the exact improvements with the AC boost method.

The inductor, used in the AC boost method and the varying frequency method, is relatively big with its volume of $2.3$ mm$^3$, compared with the piezo-electric receiver of $1.8$ mm$^3$. The extra power efficiency comes at the cost of extra volume occupied. This extra volume it occupies is probably in some applications not available. For these situations the varying frequency method without a boost converter is probably a better method. However, the drawbacks of this method should be taken into account.

For ultrasonic wireless power transfer, the acoustic path should have no big changes in acoustic impedances, as those will result in reflected power. Therefore, this powering method could only be used when no bones or air are in the acoustic path between the transmitter and the receiver. In applications where big changes in the acoustic impedances are inevitable, it could be solved by properly focusing the acoustic waves.

## 7.4. Opportunities and challenges in IC design

In this section, the opportunities and challenges involved in an IC design are discussed. Often a challenge also brings an opportunity, finding this opportunity per challenge is the goal of the section.

### 7.4.1. Design of the rectifier

The rectifier used in the comparison gives high losses because of the use of diodes. A different structure that uses controlled switches in combination with the boost switch control could improve the efficiency further.

In Figure 7.1 all current directions that are needed in the rectifier and boost switch part of the circuit are shown. A different layout solution could be researched to improve efficiency. The transistors of the rectifier could, for example, be used to implement the boost switch, see Figure 7.1. Two switches have to be designed for two way currents. However, the amount of transistors in series in the current path should be limited. A rectifier always needs two transistors in series to be able to switch both the plus and the minus. A boost-converter switch only needs one transistor in the current path.

### 7.4.2. Design of the boost converter circuit

In Section 6.4 the results are presented for the boost converter. The AC boost method suffers from the losses due to the boost converter. The gate capacitances of the switch are charged and discharged at a high frequency. This power is assumed to be lost. As is shown, at low $P_{el,av}$ the power lost at the gates is the majority of the losses.

In IC design there will be multiple transistors placed parallel to each other to make the desired transistor size. This is an opportunity because those could also be partly switched at low currents and partly held static. This could save the majority of the switching losses. Another possibility is to re-use the gate charge so the power is not fully lost.

### 7.4.3. Design of the control scheme

As is shown in Section 6.4 the implemented control is not efficient. This control could be made much more efficient if the boost converter never boosts when it could not reach the desired voltage. The proposed method is the energy based switching method: around the zero voltage point the thresholds are wider so that this energy also overcomes the barrier. This results in a less good matching but a higher power transfer. Designing this control involves knowing the inductors behaviour, the desired voltage at every moment and the losses when boosting.

### 7.4.4. Design of the current measurement

For an IC implementation the current $I_{piezo}$ and voltage $V_{piezo}$ of the piezo-electric element have to be known for the controller. The piezo-electric element, the inductor and the storage element probably have to be external components. A $V_{piezo}$ voltage measurement could be done directly but $I_{piezo}$ current measurement is currently not directly possible because there is no known method for. There are, however, multiple opportunities to measure the current indirectly in the circuit:

- **Series resistor:** a resistor in series with the piezo-electric element could be used for $I_{piezo}$ estimation with: $V_{current} = I_{piezo} \times R_{current}$. A trade-off between power loss and accuracy should be made. For $10\%$ loss of $P_{el,av}$ in $R_{current}$, $V_{current}$ is only $10\%$ of $V_{piezo}$. So the measurement accuracy of $V_{current}$ should be 10 times higher than the $V_{piezo}$ measurement to know both $V_{piezo}$ and $I_{piezo}$ with the same precision.

- **Inductor voltage:** the current through the boost converter inductor is the same as $I_{piezo}$, and could be estimated with: $V_L = L{}^{di}/_{dt}$. So the voltage $V_L$ should be measured, integrated and scaled down by $L$ to estimate $I_{piezo}$. This does not have to lead to an extra pad from the chip because $V_{piezo}$ should also be measured.

- **Inductor current copy:** using a transformer instead of an inductor enables copying a scaled down version of the inductor current, for use at the controller. This copied current should be much smaller for low losses. Such a transformer should be specifically designed and build because it is a nonstandard component.

- **boost switch current copy:** a, for example, $100$ times scaled down copy of the boost switch with the same $V_{gs}$ and $V_{ds}$ has $I_{ds} = {}^1/_{100} I_{piezo}$. This current could be used at the controller directly or measured at a resistor or integrated at a capacitor. The current is only available when the boost switch is on, so when the power is stored in the inductor. Therefore the moment of off-switching the boost switch is exactly known. The controller has to compute the moment it has to switch the boost switch on again. Another challenge is to make an exact copy of the boost switch but scaled down by a certain factor. Assuring the same $V_{gs}$ and $V_{ds}$ is also a challenge.

- **Rectifier current copy:** when the rectifier is implemented with transistors the current could be copied here as well. It could also be combined with the boost switch current copy so the current is always known.

The boost switch current copy or the rectifier current copy are the best opportunities because it is practically feasible and does not consume much power. It requires an extensive IC design but is also done often in literature.

## 7.5. Conclusion

This chapter discussed the approach used and showed that it was valid for the goal of this study. Similar results would be obtained in a future study for the theoretical reasoning, the simulation results and the final global result. The results of the AC boost method are, as expected, the best of the presented methods but not as good as it could be because of the minimal circuit design. For an IC design of the AC boost method a route with some opportunities and challenges is shown.

The following chapter will draw the main conclusions, highlight the contributions and indicate future work.

# 8

# Conclusion

In this final chapter, the final conclusions will be drawn and the main research question will be answered. This is followed by a section where the contributions of this project are highlighted. The chapter will conclude with some directions for future work.

## 8.1. Conclusions

In this study we searched for an answer to:

***Main Question**: How could maximum power transfer be achieved with wireless power transfer to a 10 cm deep implanted biomedical device?*

This question was subdivided in six questions. Every chapter answers one question.

In Chapter 2 three wireless powering methods were examined on maximum received power. The ultrasonic wireless powering method has the highest input safety limits, has least power attenuation and is most efficient at the receiver when compared with the near-field electromagnetic and far-field electromagnetic methods.

The ultrasonic wireless power transfer link is characterized in Chapter 3. The Butterworth-Van Dyke model was chosen for simulation of the wireless power link. Maximum acoustic power of $7.2$ mW/mm$^2$ was assumed at the receiver.

From the analysis of maximum power transfer and two existing methods, the AC boost method was developed in Chapter 4. The two existing methods are the standard method with no impedance transformations and the varying frequency method where the frequency is varied to change the piezo-electric element's impedance. Here two extra impedance transformations are needed.

In Chapter 5 a comparison strategy for the three methods was presented. The piezo-electric element, the rectifier and the capacitor banks that were used in the varying frequency method before [21], were used again in simulation. The boost converter and storage element were designed. LTspice is used for simulation of the three methods.

Chapter 6 presented the results of the comparison. The AC boost method is as efficient or more efficient than the other methods for a wider power range. From 20% efficiency at $10$ µW load power to 74% around 1 mW load power is possible with the chosen circuits. In the AC boost method the piezo-electric element delivers maximum power to the circuit behind it, so the method works as designed.

A discussion of these results and of the method used, and a description of the route towards a full IC design of the AC boost method are in Chapter 7.

Maximum power transfer to a tiny IMD implanted at at least 10 cm deep in the body could be achieved by using an ultrasonic wireless power transfer link with the AC boost method to boost the AC voltage, so maximum power is delivered by the piezo-electric element and maximum power could go to the DC storage element. The size requirement of $10$ mm$^3$ for the total power conversion system is met as the biggest components are:

- Piezo-electric receiver: $1.8$ mm$^3$
- Boost converter inductor: $2.3$ mm$^3$

- Storage element: $1 - 5$ mm$^3$

With the biggest storage element the total volume is thus $9.1$ mm$^3$. The volume of the boost-converter control, rectifier, and boost switch is not taken into account but probably this will be a tiny part of the IC of a complete IMD.

For IMD applications like the pancreas stimulator, ultrasonic wireless power transfer with the AC boost method gives the opportunity to design a tiny implanted device with enough available electrical power.

## 8.2. Contributions

The most important contribution is the development of the new AC boost method as it could not be found in literature. Two important steps to this new method are worth mentioning here. First, the reasoning towards the AC boost method gave the insight through the idea of waveform matching next to the well known impedance matching. This could also not be found in literature. By drawing the graphs of all important waveforms in the power conversion circuit this became clear. Secondly, a boost converter has a continuous input current and could thus be used for resistive matching. This is not a new insight but it is hardly used in literature. The route towards a full IC design is also presented so in future work this could be implemented.

The second contribution is the validation of the AC boost method. Its working is validated by performing simulations in LTspice. Maximum power is delivered by the piezo-electric element and at high efficiency the power is transferred to the storage element.

Another contribution of this thesis is the critic on the paper of the varying frequency method [21]. Some comments are made on the total efficiency that could be achieved and on the total complexity. The most important comment is, however, that the resistive load they used is unrealistic. For wireless powered IMDs there will always be fluctuations both in received and used power and thus some form of electrical storage is needed.

## 8.3. Future work

Future work for the AC boost method includes:

- **IC design:** a full IC design, tape-out and measurement should be done to prove the efficiency increase of the AC boost method. This method could not be tested with discrete components as the boost switch, current measurement and control are not available in the right specifications. A full IC design could is therefore the only way to test the AC boost method.
- **Research other applications:** the developed AC boost method could probably also be used in other applications with different AC sources, where a resistive match is a possibility and a DC voltage should be generated. A low voltage boost factor is a requirement here for high efficiency. So the impedance of the source should closely match the power requirement of the device at $1 - 2$ V. Antennas, for example, could be designed such that an antenna impedance of a few kΩ is possible at resonance frequency. Also the anti-resonance frequency could be utilized as the antenna reactance is zero here as well. However, for piezo-electric elements, the PCE is lower at the anti-resonance frequency so attention should be paid to the PCE.
- **Optimization of the piezo-electric receiver:** for bio-compatibility and the best possible parameters the piezo-electric element could be optimized.
- **Complete system design:** with the ultrasonic source outside the body and a real IMD attached to the powering circuitry a complete system could be made.
- **Testing with tissue:** for validation of the models used, a test with tissue could be performed.
- **Testing in vivo:** the ultimate test is testing the complete system in an in vivo application.
- **Implementation in an IMD application:** the final goal is the implementation in an IMD application inside the human body.

# Appendices

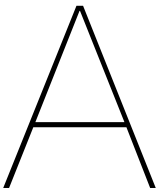

# Paper Wireless Power Transfer Conference 2019

On the following pages the accepted paper for the IEEE MTT-S Wireless Power Transfer Conference (WPTC) is included. The conference will be held during the Wireless Power Week from June 17-21, 2019, in London. The paper is accepted for an oral presentation to be held on Friday June 21st 2019. The accepted paper will be published in the conference proceedings and will also be made available online through the IEEE Xplore digital library: www.ieeexplore.ieee.org.

# Resistive Matching using an AC Boost Converter for Efficient Ultrasonic Wireless Power Transfer

Marc Bisschop
*Section Bioelectronics*
*Delft University of Technology*
Delft, The Netherlands
bisschop.mc@gmail.com

Wouter A. Serdijn
*Section Bioelectronics*
*Delft University of Technology*
Delft, The Netherlands
w.a.serdijn@tudelft.nl

***Abstract*—This paper presents a method to increase the power conversion of ultrasonic receivers in implantable medical devices. A perfect complex conjugate match between the piezo-electric receiver and the power conversion circuit is required for maximum power transfer. A boost converter in front of the rectifier enables a close to perfect resistive match. The boost converter transforms the AC voltage into a pulse width modulated square wave voltage. This saves an extra impedance transformation between the receiver and the rectifier. From circuit simulation results, it follows that this new method has the highest efficiency compared with prior art.**

***Index Terms*—impedance transformation, implantable medical devices (IMDs), maximum power transfer, resistor emulation, ultrasound, wireless power transfer.**

## I. Introduction

In implantable medical devices (IMDs), there is a need for wireless power transfer as the use of batteries has several disadvantages, the biggest one being the replacement of IMDs with fully discharged batteries. Recently, interest has been growing in ultrasound (US) wireless power transfer to implants deep inside the body (>10 cm) [1]. Ultrasound has millimeter wavelength in tissue at usable frequencies (e.g., 1.6 mm at 1 MHz) [2]. The FDA allows for a time-averaged acoustic intensity of 7.2 mW/mm$^2$ [3] and US has low attenuation in tissue (∼1 dB/MHz·cm) [1]. The impedance of an US piezo-electric receiver closely matches the power requirement of an IMD at 1-2 V [4]. These reasons enable scaling down the IMDs to millimeter sizes. Moreover, focusing of the ultrasonic waves is possible so as to ensure that the required energy will be received at the implant [5].

Little attention, however, has been paid to optimizing the electrical efficiency at the receiver and, as a consequence, much power is lost. This paper presents a design method for maximizing the usable electrical power at the IMD and proposes a new design for a close to ideal impedance match that follows from this method.

## II. Ultrasonic to Electrical Power Conversion

Piezo-electric receivers are used for converting ultrasonic waves into electric waves. Fig. 1a shows a lumped element 1D series model of an ultrasonic piezo-electric receiver around its resonance frequency in length expander mode [4]. The real part of the impedance ($R_{piezo}$) changes from 2.7 kΩ up to

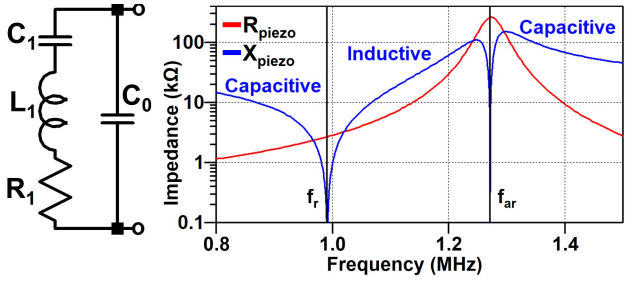


(a) (b)

Fig. 1. (a) Lumped elements 1D series model of an ultrasonic piezo-electric receiver around its resonance frequency in length expander mode. (b) impedance plot of this model for a piezo-electric element made of PZT4 and with dimensions $W = L = 1.1$ mm and $t = 1.5$ mm. Resistance $R_{piezo}$ and reactance $X_{piezo}$ are plotted. The capacitive and inductive regions are indicated.

260 kΩ over frequency for a square piezo-electric element made of PZT4 with equal width and length $W = L = 1.1$ mm and thickness $t = 1.5$ mm. See Fig. 1b. Between the resonance frequency ($f_r = 0.99$ MHz) and anti-resonance frequency ($f_{ar} = 1.27$ MHz) the reactance $X_{piezo}$ is inductive. Outside this band it is capacitive [6]. The resonance frequency and anti-resonance frequency could be calculated as follows with the material properties listed in Table I [4]:

$$f_r = \frac{v}{2t} \tag{1}$$

$$f_{ar} \simeq \sqrt{1 - \frac{8k_{33}^2}{\pi^2}} f_r \tag{2}$$

The passive circuit elements of the model are calculated as [6]:

$$C_0 = \varepsilon_0 \varepsilon_{33}^T (1 - k_{33}^2) \frac{W^2}{t} \tag{3}$$

$$C_1 = \frac{8k_{33}^2 C_0}{\pi^2 - 8k_{33}^2} \tag{4}$$

$$R_1 = \frac{1}{8k_{33}^2 f_r C_0} \frac{Z_F + Z_B}{Z_C} \tag{5}$$

$$L_1 = \frac{1}{4\pi^2 f_r^2 C_1} \tag{6}$$

TABLE I
MATERIAL PROPERTIES OF A PZT4 ELEMENT [4], [6].

| | | |
|---|---|---|
| Sound velocity | $v$ | 4100 m/s |
| Acoustic impedance | $Z_C$ | 30.8 MRayls |
| Electrical-mechanical coupling coefficient | $k_{33}$ | 0.70 |
| Relative permittivity | $\varepsilon_{33}^T$ | 1300 |
| Front acoustic impedance tissue | $Z_F$ | 1.5 MRayls |
| Back acoustic impedance air | $Z_B$ | 400 Rayls |

A perfect complex conjugate match between the impedances of the receiver and the power conversion circuit is required for maximum power transfer and preventing reflected power [7].

IMDs with wireless powering need an energy storage element due to the unreliable nature of both the received and the used power. Present IMDs, for example, are often equipped with stimulator and communication circuitry, which both consume high power for a short period of time. A rectifier is required between the piezo-electric receiver and the storage element, as electrical storage requires DC voltages. Fig. 2 shows the general block diagram of the power conversion chain of an IMD. Between all the blocks an impedance transformation should be designed to ensure optimal matching. This impedance transformation should be done both at the AC-side of the rectifier (e.g., using passive capacitors) and at the DC-side (e.g., using a boost converter).

Fig. 3 gives insight in the challenging total impedance transformation needed for maximum power transfer to the storage element. The waveform of the piezo-electric receiver voltage $V_{piezo}$ is sinusoidal and its current $I_{piezo}$ also, but smaller by a factor $R_{piezo}$. At the storage element, $V_{stor}$ is a DC voltage. The instantaneous available electrical power is:

$$P_{el}(t) = V_{piezo}(t)I_{piezo}(t) \quad (7)$$
$$= V_{stor}(t)I_{stor}(t)\eta_{total} \quad (8)$$

where $\eta_{total}$ is the total power efficiency of the power conversion system, in the ideal case equal to 1, and $I_{stor}$ is the current into the storage element. For a constant $\eta_{total}$ and a DC $V_{stor}$, the $I_{stor}$ waveform is thus similar to the $P_{el}$ waveform: a squared sinus. Consequently, the signal requires significant processing for maximum power transfer.

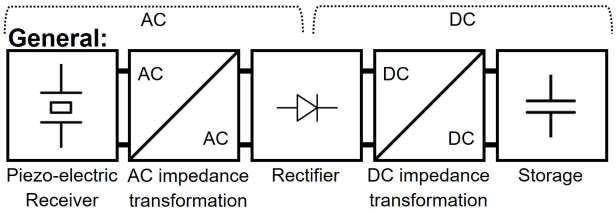


Fig. 2. General block diagram of ultrasonic wireless power transfer to an energy storage element.

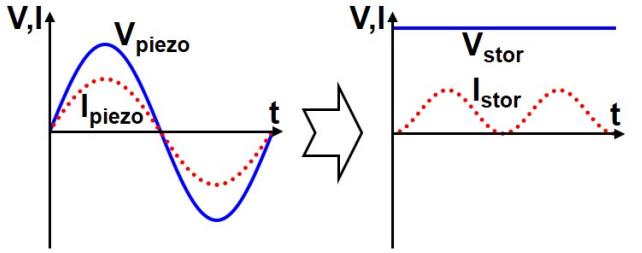


Fig. 3. $V_{piezo}$ and $I_{piezo}$ waveforms of a piezo-electric element operating at resonance frequency for maximum power transfer, and the $V_{stor}$ and $I_{stor}$ waveforms when the full $P_{el}$ is transferred through the power conversion chain.

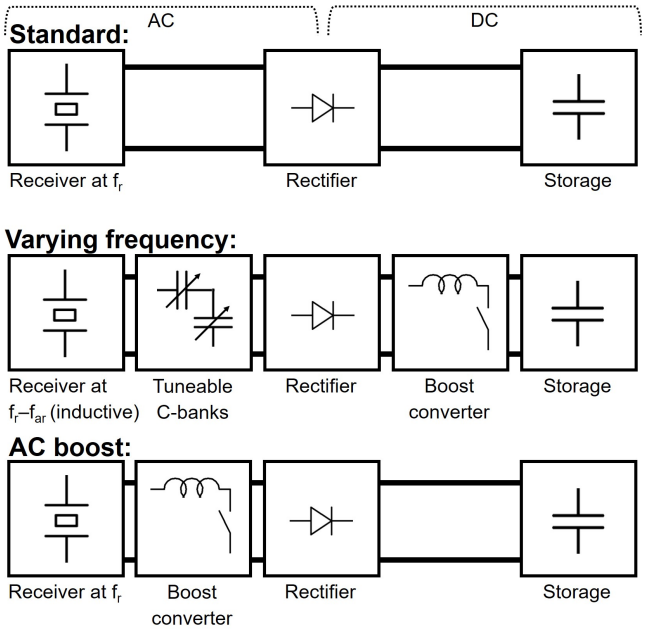


Fig. 4. Block diagrams of the three methods based on the general block diagram of Fig. 2. Standard method: without extra impedance transformations. Varying frequency method: vary across inductive band with tunable capacitor banks and DC boost converter. AC boost method: with AC boost converter operating as resistor emulation.

## III. DESIGN METHODS FOR MAXIMUM POWER CONVERSION

A power conversion chain, based on the general block diagram of Fig. 2, that produces the ideal waveforms of Fig. 3 is difficult to implement as it should continuously change the matching transformation factor. However, there are methods that make it possible to design a system that produces the waveforms close to the ideal waveforms. In Fig. 4, three methods of power conversion are shown. All have a passive rectifier and a storage element so the concepts are orthogonal in itself and comparable with each other. Conventional methods are the standard method and the varying frequency method, whereas the proposed method is the AC boost method.

### A. Standard: no impedance transformations

This is the basic method that is widely used, e.g., in [8]. Much of the power is lost because the current will flow only

if the AC voltage $V_{piezo}$ is larger than the voltage needed to turn on the rectifier, which is $V_{stor}$ plus the voltage drop of the rectifier. So every cycle at least some power is lost. This solution does not efficiently handle large power fluctuations, since these induce impedance mismatches.

### *B. Varying frequency: vary across inductive band with tuneable capacitor bank*

This method is applied in, e.g., [4]. By increasing the frequency at low acoustic power $P_a$, $R_{piezo}$ increases. The peak open-circuit voltage of the piezo-electric receiver is therefore constant [8]:

$$V_{oc} = \sqrt{8 \cdot PCE \cdot P_{a,av} \cdot R_{piezo}} = \sqrt{8 \cdot P_{el,av} \cdot R_{piezo}} \quad (9)$$

where $PCE$ is the power conversion efficiency of the piezo-electric receiver, and $P_{a,av}$ and $P_{el,av}$ are the average acoustic and electrical power, respectively.

Tuneable capacitor banks compensate for the varying inductive behaviour, which gives an increase in efficiency but has some disadvantages. Since the frequency needs to be tunable, there has to be constant communication from the IMD back to the acoustic sender about the received power, to close the control loop. This communication has a delay so the frequency and power level could only be adjusted after some cycles, resulting in a less optimal match. Further, for PZT4 material, the PCE is highest ($\sim 1$) at $f_r$; at higher frequencies the PCE drops (to $\sim 0.5$) and the losses in tissue are higher as well.

In [4] no storage element is used. For comparability, we add a storage element to the concept and, for efficiency, a boost converter is added at the storage side of the rectifier.

### *C. AC boost: boosting the AC voltage*

The method proposed here uses an AC boost converter at the receiver side of the rectifier. At high switching frequencies ($f_{sw} \gg f_r$), the receiver voltage $V_{piezo}$ is boosted to a higher voltage $V_{boost}$, so all power can overcome the voltage barrier of the rectifier and storage element. The voltage waveform in front of the rectifier is transformed into a pulse width modulated square wave. An advantage of the boost topology is the continuous input current as is required for proper impedance matching. Another advantage is the ability to adjust the matching factor immediately, ensuring a close to ideal match.

## IV. Design of AC boost: resistor emulation

To realize the maximum power transfer theorem the following relation should be implemented by the circuit when the receiver is operating at its resonance frequency:

$$I_{piezo} = V_{piezo}/R_{piezo} \quad (10)$$

where $V_{piezo}$ is half of $V_{oc}$ to achieve maximum power transfer. Fig. 5a shows an implementation of this concept. The current through $L_{boost}$ ($I_{piezo}$) is controlled by a feedback loop with two comparators that operate the switch when it crosses the threshold values. For a situation with ideal components the result is plotted in Fig. 5b, where $I_{piezo}$ is allowed to be between the threshold values of 0.8 and 1.2 times the ideal current curve. The current follows the voltage, hence (10) is fulfilled, so a close to ideal match is continuously made, ensuring maximum power transfer.

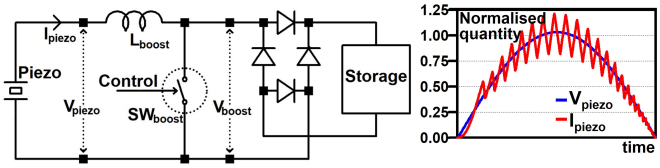


(a) (b)

Fig. 5. (a) AC Boost converter at the receiver side of the rectifier for resistor emulation. (b) Simulation of the ideal resistor emulation. The normalized $V_{piezo}$ and $I_{piezo}$ are plotted. The current follows the curve of the voltage so there is always a close power match.

To prove the increase in power transfer, components with realistic circuit models are used in a circuit simulation. The piezo-electric receiver is made from PZT4, has a 987 kHz resonance frequency with power conversion efficiency 1.0, is 1.5 mm thick and 1.1 mm wide and long. The maximum available electrical power is 8.71 mW. Its impedance is plotted in Fig. 1b [4]. The real inductor has an inductance of 100 $\mu$H, a typical self-resonance frequency of 13 MHz ($\sim f_{sw}$), a maximum DC resistance of 12.25 $\Omega$ and a volume of 2.3 mm$^3$ (Coilcraft XFL2006-104ME). Two NMOS transistors, composed of 3 parallel 500 nm $\times$ 20 $\mu$m devices, operating as a bidirectional switch are designed in a standard 500 nm technology, with the technology parameters from [9]. The sizes of the switches are a trade-off between the on-resistance and the gate capacitance. The power needed to operate the switches is assumed to be lost. The voltages in the circuit are all in the allowed range of the 500 nm technology. No blocking diode is needed in the boost converter because the rectifier blocks reverse currents. The rectifier is a schottky RF rectifier (Avago HSMS282X). We assume a capacitor as the storage element, which is charged to 2 V as this is well above the transistor threshold voltage and within the specifications of current IMDs and IC technology. The same piezo-electric receiver and rectifier are also used in [4], enabling a comparison of power efficiency.

## V. Efficiency comparison of the three concepts

The three methods are simulated with the components of the previous section. The standard method is simulated without a boost converter. For the varying frequency method the components at the AC-side, i.e. the piezo-electric element, the tuneable capacitor bank and the rectifier, are not simulated but the efficiency results are taken from [4]. These efficiency results are multiplied with the boost converter efficiency for every power level. An ideal blocking diode is added to the boost converter in the varying frequency method because no rectifier follows the boost converter. The extra losses of the continuous communication for frequency adjustment and control of the capacitor banks in the varying frequency method are not taken into account and zero communication delay

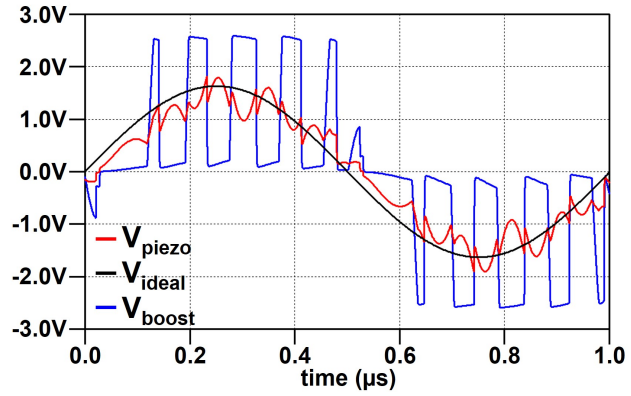


Fig. 6. Simulation results of the AC boost method for $P_{el,av} = 0.5$ mW. Plotted are the ideal $V_{piezo}$ together with the simulated $V_{piezo}$. The AC boost voltage is also plotted.

is assumed so a match is made without delay. The allowed current range thresholds are optimized for maximum power transfer for both the varying frequency method and the AC boost method.

The voltage waveforms in the AC boost method are plotted in Fig. 6 for $P_{el,av} = 0.5$ mW. $V_{piezo}$ is always close to the ideal sinusoidal voltage waveform here, providing nearly maximum power delivery by the piezo-electric receiver. The AC voltage is boosted high enough to overcome the voltage barrier of the rectifier and storage element. Sometimes the voltage is not boosted high enough because not enough energy is stored in the inductor at that moment. The control, however, does operate the switch since it does not estimate the energy stored in the inductor.

Fig. 7 shows the simulation results of the power efficiency of the three methods. The AC boost method is for the full power range the most efficient method, around $P_{load} = 1$ mW the efficiency is 74% and this drops to 22% at $P_{load} = 0.01$ mW. At $P_{load} = 2$ mW the standard method is also 74% efficient but for different power levels the efficiency is much lower, at $P_{load} = 0.1$ mW the efficiency has already dropped to 23%. The varying frequency method is as efficient as the AC boost method from $P_{load} = 0.01$ mW to $P_{load} = 0.1$ mW, but for higher power levels the efficiency is lower than the AC boost method.

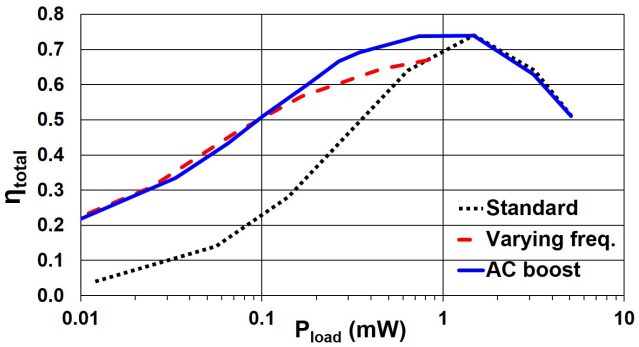


Fig. 7. Simulation results of the power efficiency as a function of load power for the three methods.

## VI. Discussion and Conclusions

In this paper it has been shown that, for maximum power transfer in ultrasonic wireless powering of IMDs, the impedance of the receiver has to be complex conjugate matched to the power conversion circuit. For this, two impedance transformations are needed, one at the receiver side of the rectifier and one at the storage side of the rectifier. The standard method without added impedance transformations is the least efficient as expected. The varying frequency method with tunable capacitor banks, as proposed in [4], is more efficient but has some drawbacks: fully tunable capacitor banks are required, continuous communication is needed, which has a delay and consumes power, and extra losses occur both in the tissue and the receiver. The AC boost method with a boost converter at the AC-side, as proposed here, enables resistive impedance matching over a wide output power range and has the highest power efficiency. It requires only one impedance transformation, viz. the boost converter.

The proposed method can be further improved by making a full IC design of this concept. The rectifier could be made of active components and synchronized with the boost switch. The control could also be improved by implementing an energy estimation so that the switch only closes when the inductor has enough energy to overcome the rectifier turn-on voltage and charge the storage element.

## References

[1] A. Denisov and E. Yeatman, "Ultrasonic vs. inductive power delivery for miniature biomedical implants," in *Body Sensor Networks (BSN), 2010 International Conference on*. IEEE, 2010, pp. 84–89.

[2] C. R. Hill, J. C. Bamber, and G. R. ter Haar, *Physical principles of medical ultrasonics*, 2nd ed. John Wiley & Sons, Ltd, 2004.

[3] U.S. Food and Drug Administration, "Information for manufacturers seeking marketing clearance of diagnostic ultrasound systems and transducers," *Rockville, MD, USA: Center for Devices and Radiological Health*, 2008.

[4] T. C. Chang, M. J. Weber, M. L. Wang, J. Charthad, B. P. T. Khuri-Yakub, and A. Arbabian, "Design of tunable ultrasonic receivers for efficient powering of implantable medical devices with reconfigurable power loads," *IEEE transactions on ultrasonics, ferroelectrics, and frequency control*, vol. 63, no. 10, pp. 1554–1562, 2016.

[5] F. Mazzilli, C. Lafon, and C. Dehollain, "A 10.5 cm ultrasound link for deep implanted medical devices," *IEEE transactions on biomedical circuits and systems*, vol. 8, no. 5, pp. 738–750, 2014.

[6] G. S. Kino, *Acoustic waves: devices, imaging, and analog signal processing - Prentice-Hall Signal Processing Series*. Englewood Cliffs, Prentice-Hall, 1987.

[7] M. Stoopman, Y. Liu, H. J. Visser, K. Philips, and W. A. Serdijn, "Codesign of electrically short antenna–electronics interfaces in the receiving mode," *IEEE Transactions on Circuits and Systems II: Express Briefs*, vol. 62, no. 7, pp. 711–715, 2015.

[8] M. J. Weber, A. Bhat, T. C. Chang, J. Charthad, and A. Arbabian, "A miniaturized ultrasonically powered programmable optogenetic implant stimulator system," in *2016 IEEE Top. Conf. Biomed. Wirel. Technol. Networks, Sens. Syst*, 2016, pp. 12–14.

[9] B. Razavi, *Design of analog CMOS integrated circuits*, 2nd ed. McGraw-Hill Education, 2017.

# Bibliography


[1] V. Giagka and W. A. Serdijn, "Realizing flexible bioelectronic medicines for accessing the peripheral nerves–technology considerations," *Bioelectronic Medicine*, vol. 4, no. 1, p. 8, 2018.

[2] S. Rao and J.-C. Chiao, "Body electric: Wireless power transfer for implant applications," *IEEE Microwave Magazine*, vol. 16, no. 2, pp. 54–64, 2015.

[3] A. Denisov and E. Yeatman, "Ultrasonic vs. inductive power delivery for miniature biomedical implants," in *Body Sensor Networks (BSN), 2010 International Conference on*. IEEE, 2010, pp. 84–89.

[4] J. Charthad, M. J. Weber, T. C. Chang, and A. Arbabian, "A mm-sized implantable medical device (imd) with ultrasonic power transfer and a hybrid bi-directional data link," *IEEE Journal of Solid-State Circuits*, vol. 50, no. 8, pp. 1741–1753, 2015.

[5] X. Wei and J. Liu, "Power sources and electrical recharging strategies for implantable medical devices," *Frontiers of Energy and Power Engineering in China*, vol. 2, no. 1, pp. 1–13, 2008.

[6] M. Clinic, "Pancreatic cancer - overview," https://www.mayoclinic.org/diseases-conditions/pancreatic-cancer/symptoms-causes/syc-20355421, 2019, accessed: 2019-03-14.

[7] H. Divanović, D. Mulić, A. Padalo, E. Rastoder, Š. Pedljak, N. Žiga, and T. Bego, "Effects of electrical stimulation as a new method of treating diabetes on animal models," in *CMBEBIH 2017*. Springer, 2017, pp. 253–258.

[8] J. Rozman, B. Zorko, M. Bunc, and M. Žitko, "Stimulation of nerves innervating the dog's pancreas," *Artificial organs*, vol. 26, no. 3, pp. 241–243, 2002.

[9] M. G. Roes, J. L. Duarte, M. A. Hendrix, and E. A. Lomonova, "Acoustic energy transfer: A review," *IEEE Transactions on Industrial Electronics*, vol. 60, no. 1, pp. 242–248, 2013.

[10] K. Agarwal, R. Jegadeesan, Y.-X. Guo, and N. V. Thakor, "Wireless power transfer strategies for implantable bioelectronics: Methodological review," *IEEE Reviews in Biomedical Engineering*, 2017.

[11] IEEE, "IEEE Standard for Safety Levels with Respect to Human Exposure to Radio Frequency Electromagnetic Fields, 3 kHz to 300 GHz," *IEEE Std C95.1-2005 (Revision of IEEE Std C95.1-1991)*, pp. 1–238, April 2006.

[12] U.S. Food and Drug Administration, "Information for manufacturers seeking marketing clearance of diagnostic ultrasound systems and transducers," *Rockville, MD, USA: Center for Devices and Radiological Health*, 2008.

[13] D. Seo, J. M. Carmena, J. M. Rabaey, E. Alon, and M. M. Maharbiz, "Neural dust: An ultrasonic, low power solution for chronic brain-machine interfaces," *arXiv preprint arXiv:1307.2196*, 2013.

[14] K. Van Schuylenbergh and R. Puers, *Inductive powering: basic theory and application to biomedical systems*. Springer Science & Business Media, 2009.

[15] C. R. Hill, J. C. Bamber, and G. R. ter Haar, *Physical principles of medical ultrasonics*, 2nd ed. John Wiley & Sons, Ltd, 2004.

[16] J. S. Ho, S. Kim, and A. S. Poon, "Midfield wireless powering for implantable systems," *Proceedings of the IEEE*, vol. 101, no. 6, pp. 1369–1378, 2013.

[17] G. S. Kino, *Acoustic waves: devices, imaging, and analog signal processing - Prentice-Hall Signal Processing Series*. Englewood Cliffs, Prentice-Hall, 1987.

[18] A. Arbabian, T. C. Chang, M. L. Wang, J. Charthad, S. Baltsavias, M. Fallahpour, and M. J. Weber, “Sound technologies, sound bodies: Medical implants with ultrasonic links,” *IEEE Microwave Magazine*, vol. 17, no. 12, pp. 39–54, 2016.

[19] F. Mazzilli, C. Lafon, and C. Dehollain, “A 10.5 cm ultrasound link for deep implanted medical devices,” *IEEE transactions on biomedical circuits and systems*, vol. 8, no. 5, pp. 738–750, 2014.

[20] H. Azhari, *Basics of biomedical ultrasound for engineers*. John Wiley & Sons, 2010.

[21] T. C. Chang, M. J. Weber, M. L. Wang, J. Charthad, B. P. T. Khuri-Yakub, and A. Arbabian, “Design of tunable ultrasonic receivers for efficient powering of implantable medical devices with reconfigurable power loads,” *IEEE transactions on ultrasonics, ferroelectrics, and frequency control*, vol. 63, no. 10, pp. 1554–1562, 2016.

[22] D. M. Pozar, *Microwave engineering*, 4th ed. John Wiley & Sons, Inc., 2012.

[23] S. Sherrit, S. P. Leary, B. P. Dolgin, and Y. Bar-Cohen, “Comparison of the mason and klm equivalent circuits for piezoelectric resonators in the thickness mode,” in *1999 IEEE Ultrasonics Symposium. Proceedings. International Symposium (Cat. No. 99CH37027)*, vol. 2. IEEE, 1999, pp. 921–926.

[24] J. Kim, B. L. Grisso, J. K. Kim, D. S. Ha, and D. J. Inman, “Electrical modeling of piezoelectric ceramics for analysis and evaluation of sensory systems,” in *2008 IEEE Sensors Applications Symposium*. IEEE, 2008, pp. 122–127.

[25] M. J. Weber, A. Bhat, T. C. Chang, J. Charthad, and A. Arbabian, “A miniaturized ultrasonically powered programmable optogenetic implant stimulator system,” in *2016 IEEE Topical Conference on Biomedical Wireless Technologies, Networks, and Sensing Systems (BioWireleSS)*. IEEE, 2016, pp. 12–14.

[26] M. Dürr, A. Cruden, S. Gair, and J. McDonald, “Dynamic model of a lead acid battery for use in a domestic fuel cell system,” *Journal of power Sources*, vol. 161, no. 2, pp. 1400–1411, 2006.

[27] C. Bowick, *RF circuit design*. Elsevier, 1982.

[28] A. K. Rohit, K. P. Devi, and S. Rangnekar, “An overview of energy storage and its importance in indian renewable energy sector: Part i–technologies and comparison,” *Journal of Energy Storage*, vol. 13, pp. 10–23, 2017.

[29] M. Hannan, M. Hoque, A. Mohamed, and A. Ayob, “Review of energy storage systems for electric vehicle applications: Issues and challenges,” *Renewable and Sustainable Energy Reviews*, vol. 69, pp. 771–789, 2017.

[30] *HSMS-282X Surface Mount RF Schottky Barrier Diodes*, Avago Technologies, 2014.

[31] *Shielded Power Inductors XFL2006*, Coilcraft, 2018.

[32] B. Razavi, *Design of analog CMOS integrated circuits*, 2nd ed. McGraw-Hill Education, 2017.

[33] Analog Devices, “Design center - LTspice,” https://www.analog.com/en/design-center/design-tools-and-calculators/ltspice-simulator.html, 2019, accessed: 2019-05-09.